Analytical study of von Kármán swirling flow involving viscoelastic fluids

by

Muhammad Burhan Jafeer

A dissertation submitted in partial fulfillment of the requirements
for the degree of Master of Philosophy in Mathematics

Supervised by

Dr. Meraj Mustafa Hashmi

School of Natural Sciences

National University of Sciences and Technology
Islamabad, Pakistan

FORM TH-4

National University of Sciences & Technology

MS THESIS WORK

We hereby recommend that the dissertation prepared under our supervision by: Muhammad Burhan Jafeer, Regn No. 00000203167 Titled: Analytical study of von Kármán swirling flow involving viscoelastic fluids accepted in partial fulfillment of the requirements for the award of **MS** degree.

Examination Committee Members

1. Name: DR. MUHAMMAD ASIF FAROOQ   Signature: _____

2. Name: DR. MUJEEB UR REHMAN   Signature: _____

External Examiner: DR. ZAHID IQBAL   Signature: _____

Supervisor's Name DR. MERAJ MUSTAFA HASHMI   Signature: _____

_____
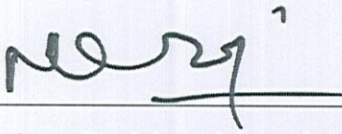Head of Department

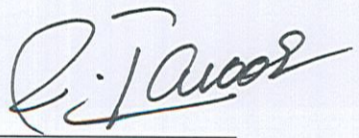28/07/2020
Date

COUNTERSINGED

Date: 28/7/2020

Dean/Principal

THESIS ACCEPTANCE CERTIFICATE

Certified that final copy of MS thesis written by **Mr. Muhammad Burhan Jafeer** (Registration No. **00000203167**), of **School of Natural Sciences** has been vetted by undersigned, found complete in all respects as per NUST statutes/regulations, is free of plagiarism, errors, and mistakes and is accepted as partial fulfillment for award of MS/M.Phil degree. It is further certified that necessary amendments as pointed out by GEC members and external examiner of the scholar have also been incorporated in the said thesis.

Signature: _____

Name of Supervisor: Dr. Meraj Mustafa Hashmi

Date: _____28/07/2020_____

Signature (HoD): _____T.F._____

Date: _____28/07/2020_____

Signature (Dean/Principal): _____

Date: _____28/7/2020_____

Dedication

This study is dedicated to my loving parents

for their never-ending love, prayers & support.

Acknowledgments

Table of contents

List of figures

List of tables

Abstract

This thesis presents mathematical framework for von-Karman flow of viscoelastic fluids namely second grade fluid and Walters B liquid. Here particular interest is to resolve resulting heat transfer problems when viscous dissipation terms are included. Computational analysis is based on the assumption that temperature at the disk is distributed quadratically. Such an assumption is indeed important for the governing problem to exhibit a self-similarity solution. Arising self-similar system is solved by package BVPh2.0 which is based upon renowned homotopy analysis method (HAM). Averaged squared residuals of series solutions are worked out and optimal values of the auxiliary parameters are found. These findings demonstrate the approximate solutions approach the exact solutions upon enhancing the order of approximation. The consequence that viscous dissipation can have on the considered models is scrutinized through graphical and numerical data. Significant fluid dynamics concept such as skin friction coefficients, minimum torque requirement, heat transfer rates, volumetric flow rate etc. are thoroughly investigated from the derived analytical solutions.

.

Chapter 1

Introduction

This section consists of few definitions and core concepts related to heat transfer and flow of fluid. For flow problems highlighted in subsequent chapters, a comprehensive yet precise literature survey is presented. Finally, the analytical procedure adopted in this thesis is described for a selected flow model.

1.1   Newtonian versus non-Newtonian fluids

Fluids are mainly categorized as Newtonian and non-Newtonian based on how they react to the effect of applied shear stress. Different from the usual Newtonian fluids such as air and water, stress-strain curve of non-Newtonian fluids does not contain origin in general. Newtonian fluid theory, on one side, is good enough to explain the evolutional behavior of moving fluids like water, organic solvents, honey and many thin oils. On the other hand, it is unable to explain certain physical phenomena such as the Merrington effect, Weissenberg effect, normal effect and centrifugal pump effect, etc.

The frequent and broad occurrence of non-Newtonian behavior in diverse applications (both in nature and technology) is well established. Past researches summarized how non-Newtonian fluid flow is beneficial in some industrial processes including fluid friction reduction, surfactant applications for cooling/heating of large buildings and use of polymer additives to improve flow in petroleum pipe lines. Non-Newtonian behavior is also met in mining industry which treats slurries and mud, and in applications such as lubrication and biomedical flows. In most of the industrial processes, the Newtonian fluid assumption stands invalid and a complex non-Newtonian response needs to be modeled. Some of the examples of such fluids are coal oil slurries, clay-coating, shampoo, soap, coal water, lubricants, cosmetic products and glues. These fluids are widely categorized as visco-elastic, time independent and time dependent in nature. Time-dependent fluids are not only dependent upon the applied shear stress but also upon the time for which stress is being applied whereas time independent fluids behave otherwise. Out of various categories of non-Newtonian fluids there are those representing viscoelastic nature, because of their ability to possess a certain degree of elasticity besides viscosity.

1.2   Constitutive equations of viscoelastic fluids

Viscoelastic fluids show properties of both viscosity and elasticity upon deformation. These fluids, upon motion, absorb a certain amount of energy called strain energy whereas viscous dissipation also causes some of the energy to lose. The strain energy forces the fluid to regain its original shape which it could not acquire wholly because of some energy loss. This lag quantifies the degree of being elastic which is also known as the memory of fluid. The identification of normal stresses in simple shear flows is an indicator of elastic response in fluids. These stresses in simple shear flows are described as $N_1 = \sigma_{11} - \sigma_{22}$ and $N_2 = \sigma_{22} - \sigma_{33}$, also called first ($N_1$) and second ($N_2$) normal stress differences. The viscoelastic fluid models that we have selected for our study are second grade fluid and Walter's B liquid (with short memory).

1.2.1 Second grade fluid

Rivlin and Ericksen [1] proposed following stress tensor for viscoelastic fluids:

$$\boldsymbol{\tau} = -p\mathbf{I} + \mu\mathbf{A_1} + \alpha_1\mathbf{A_2} + \alpha_2\mathbf{A_1^2}, \tag{1.1}$$

where p stands for pressure, $\mu \geq 0$ is the viscosity coefficient, α_1, α_2 are material parameters of second grade fluid obeying the constraint $\alpha_1 + \alpha_2 = 0$ and $\mathbf{A_1}$ and $\mathbf{A_2}$ are first and second Rivlin-Ericksen tensors defined below

$$\mathbf{A_1} = \nabla\mathbf{v} + (\nabla\mathbf{v})^t, \tag{1.2a}$$

$$\mathbf{A_2} = \frac{d\mathbf{A_1}}{dt} + \mathbf{A_1}\nabla\mathbf{v} + (\nabla\mathbf{v})^t\mathbf{A_1}, \tag{1.2b}$$

where $\mathbf{v}$ is velocity vector.

1.2.2 Walters B liquid

Walters [2] proposed the following Cauchy stress tensor $\boldsymbol{\tau}$ for elastico-viscous fluids:

$$\boldsymbol{\tau} = -p\mathbf{I} + \eta_0\mathbf{A_1} - \kappa_0\frac{D\mathbf{A_1}}{Dt}, \tag{1.3}$$

where η_0 stands for apparent viscosity, κ_0 is termed material fluid parameter, $\mathbf{I}$ represents identity tensor and $D\mathbf{A_1}/Dt$ denotes the upper-convected time derivative of first Rivlin Ericksen tensor $\mathbf{A_1}$ defined below:

$$\frac{D\mathbf{A_1}}{Dt} = \frac{d\mathbf{A_1}}{dt} - (\nabla\mathbf{v})\mathbf{A_1} - \mathbf{A_1}(\nabla\mathbf{v})^t. \tag{1.4}$$

where **v** is a velocity vector.

1.3 Basic definitions and concepts

1.3.1 Compressible versus incompressible flows

In response to a pressure change, the flow behavior of a fluid can be categorized as being compressible or incompressible in nature. The density of fluid remains invariant for incompressible flows whereas it (density) varies spatially in the flow field in case of compressible flows. The Mach number (a dimensionless entity used to characterize the compressibility of fluid flow problems) of the fluid is less than 0.3 for incompressible flows whereas it is greater than 0.3 for compressible flows.

1.3.2 Steady versus unsteady flows

In steady flow regime, all of the fluid flow parameters (i.e. velocity, pressure, density, etc.) exhibit invariance over time at any point in the field. On the other hand, unsteady flows show dependence of time for all of its fluid properties. Mathematically, steady and unsteady flows can be expressed as $\partial \phi / \partial t = 0$ and $\partial \phi / \partial t \neq 0$ respectively where ϕ symbolizes any fluid property.

1.3.3 Laminar versus turbulent flows

The flow pattern where each particle smoothly follows its own path in a particular layer with no layers crossing one another is known as laminar flow. Turbulent flow, on the other hand, is the fluid flow where fluid particles fail to move in an orderly manner and adjacent layers cross one another. The laminar flow is noticed for viscous fluids having low Reynolds number (<1000) whereas fluids having low viscosity and high Reynolds number (>10,000) exhibit turbulent flow pattern.

1.4 Conservation laws

The analysis of a fluid dynamics problem usually involves working out the velocity field to describe the flow pattern. The fluid in motion must satisfy the fundamental principles of mechanics (laws of mass, momentum and energy conservation), a constitutive relation and associated boundary conditions.

1.4.1 Mass conservation law

The law of mass conservation states that, amount of mass entering and leaving a fixed area (control volume) remains conserved. De facto, the accumulation of mass within a control volume solely relies upon net mass inflow (by assuming zero internal sources). Mathematically, it can be translated as

$$\frac{\partial \rho}{\partial t} + \nabla \cdot (\rho \mathbf{v}) = 0, \tag{1.5}$$

where ρ is density, $\mathbf{v}$ is termed velocity whereas ∇ is defined as the gradient operator. For an incompressible fluid, Eq. (1.5) gets simplified and reduces to

$$\nabla \cdot \mathbf{v} = 0. \tag{1.6}$$

1.4.2 Momentum conservation law

In fluid mechanics, this law is stated as, the sum of all forces acting on a control volume is equal to the time rate of change of linear momentum (of contents inside control volume) and net outflow of linear momentum via mass (out of control surface). Mathematically;

$$\rho \frac{d\mathbf{v}}{dt} = \nabla \cdot \boldsymbol{\tau} + \rho \mathbf{b}, \tag{1.7}$$

where $\boldsymbol{\tau}$ is stress tensor $\mathbf{b}$ is defined as body force per unit mass of the fluid and d/dt is the material-time derivative.

1.4.3 Energy conservation law

The energy conservation law is translated as, the rate of increase in the sum of kinetic and internal energies inside a control volume must equal the rate of energy addition (via heat conduction and flow) and the rate at which the fluid (outside control volume) is doing work on the fluid inside control volume. Mathematically, it can be expressed as

$$\rho C_p \frac{DT}{Dt} = \kappa \nabla^2 T + \mu \Phi, \tag{1.8}$$

where C_p symbolize specific heat capacity at constant pressure, κ denotes the thermal conductivity of fluid whereas $\Phi = \tau_{ij} \, \partial u_i / \partial x_j$ is known as dissipation function, defined in cylindrical coordinates as

$$\Phi = \tau_{rr}\left(\frac{\partial u}{\partial r}\right) + \tau_{r\varphi}\left(\frac{\partial v}{\partial r} - \frac{v}{r}\right) + \tau_{rz}\left(\frac{\partial u}{\partial z} + \frac{\partial w}{\partial r}\right) + \tau_{\varphi\varphi}\left(\frac{u}{r}\right) + \tau_{\varphi z}\left(\frac{\partial v}{\partial z}\right) + \tau_{zz}\left(\frac{\partial w}{\partial z}\right). \tag{1.9}$$

1.5   Boundary layer

Prandtl put forward a theory in his paper about motion of fluids with very little friction that the frictional effects make the fluid directly in contact with the surface to adhere to the surface (i.e. no slip condition) and the effects of friction are felt by the fluid only in a small region called boundary layer. He has revolutionized the way scientists conceptualize fluid dynamics and quantitative measure of skin friction drag is an aftermath of his theory.

In order to get an insight into the concept, Fig. 1.1 is sketched which exhibits the boundary layer formulation over a stationary flat plate. The velocity of the fluid can be observed to vary from zero velocity at bounding surface to free stream velocity outside boundary layer.
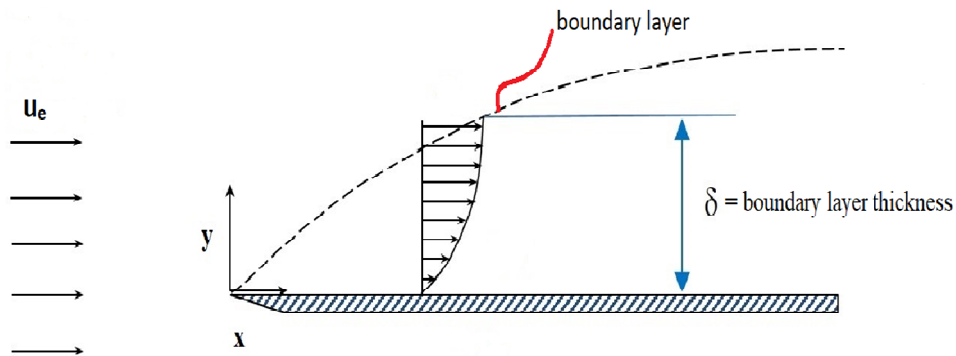
Fig. 1.1: Boundary layer over a flat plate

1.6   Non dimensionalization

The removal of dimensions from system via rescaling of variables basically is a technique to reduce the complexity and number of variables (governing the dynamics of a problem) and then grouping them into dimensionless, unit-less, forms. The solution of a dimensionless equation obtained by reducing the number of independent variables of a governing equation using coordinate transformations is called a similarity solution.

It is a well known fact that the governing equations of fluid flow are extremely difficult to analyze, so we divert our attention towards transforming them in the most efficient form possible in order to increase the usefulness of the obtained solutions. This task is accomplished by non-dimensionalization of governing equations as well as boundary conditions, thereby providing lesser number of flow parameters.

Out of many, one side benefit of this technique is the provision of scaling laws for the problem which helps in conversion of data from a small model to a large prototype. The non-dimensionalization of the governing equations not only provides information about the underlying physical phenomena but also indicates the dominating forces. For instance, the two differently scaled flows having similar geometry (a model and a prototype) satisfying the basic equations of fluid motion would only produce the same results if these flows had same values for all of the dimensionless parameters (i.e. the relative importance of the forces is same).

1.6.1 Reynolds number

The dimensionless parameter Re quantifies the ratio of inertial and viscous forces and it is used to characterize the fluid flow to be either laminar or turbulent. The laminar flow is observed at low Reynolds number which physically means the dominance of viscous forces. On the other hand, at higher values of Reynolds number, the inertial force dominate and flow is observed to be turbulent. Mathematically, it is expressed as:

$$Re = \frac{Inertial\ force}{Viscous\ force} = \frac{vL}{v},$$
(1.10)

where v and L is the velocity and characteristic length of the fluid and $v = \rho/\mu$ is the kinematic viscosity of the fluid.

1.6.2 Magnetic interaction parameter

The magnetic interaction parameter is the ratio of Lorentz force to that of inertial force. As the name suggests, it tells us the relative importance of magnetic force versus the force produced by the momentum of fluid. The dominance of Lorentz force is apparent (i.e. fluid's velocity decreases) for higher values of magnetic interaction parameter. Mathematically, it can be stated as

$$M = \frac{Lorentz\ force}{Inertial\ force} = \frac{\sigma B_0^2}{\rho\omega},$$
(1.11)

where B_0 and σ are defined as magnetic field strength and electrical conductivity of the fluid respectively.

1.6.3 Eckert number

Eckert number Ec is defined as the ratio of kinetic energy to enthalpy which is used to characterize the effect of self-heating of a fluid as a consequence of dissipation effects. Mathematically, it is expressed as

$$Ec = \frac{Kinetic\ Energy}{Enthalpy} = \frac{v^2}{C_p \Delta T},$$ (1.12)

where v is termed as fluid's average velocity and ΔT is defined as the temperature difference.

1.6.4 Nusselt number

The Nusselt number Nu is a quantitative measure of convective to conductive heat transfer and it is equivalent to non dimensional temperature gradient at the surface. The effect of Nusselt number to temperature boundary layer is analogous to the effect of skin friction coefficient for the velocity boundary layer. It is defined as

$$Nu = \frac{Convective\ heat\ transfer}{Conductive\ heat\ transfer} = \frac{hL}{\kappa},$$ (1.13)

where L denotes the characteristic length, κ denotes the thermal conductivity and h represents convective heat transfer coefficient of the fluid.

1.6.5 Prandtl number

The Prandtl number Pr is defined as the ratio of viscous diffusion rate to that of thermal diffusion rate which is used to characterize relative thicknesses of momentum and thermal boundary layers. It is independent of any flow property and depends only upon the material under consideration. It is represented, mathematically, as

$$Pr = \frac{v}{\alpha} = \frac{Viscous\ diffusion\ rate}{Thermal\ diffusion\ rate} = \frac{C_p \mu}{\kappa},$$ (1.14)

where C_p represents specific heat capacity and α symbolizes thermal diffusivity of the fluid.

1.7   Literature review

Non-Newtonian flow behavior is met in different chemical and allied processing applications. Fluids that are used in industries such as motor oil, polymer melts,, emulsions, slurries and solutions, etc. show non-Newtonian effects i.e. the stress to strain curve of these fluids does not

pass through origin in general. A subdivision of non-Newtonian liquids include those exhibiting memory effects, which are termed viscoelastic fluids. In such fluids, fluid motion is not only described by the present stress state but also by the strain history of volume element. Second grade model has been widely considered to analyze viscoelastic effects in numerous boundary layer problems. Using a perturbation approach, Rajagopal et al. [3] addressed boundary layer development over a stretchable surface in a viscoelastic fluid obeying second grade model. Later, an exact solution for thermal transport in viscoelastic fluid residing over a stretchable surface was furnished by Dandapat and Gupta [4]. These brilliant works clearly depicted that resulting boundary layer thickness was markedly affected by elasticity effects. With such motivation, Sarma and Rao [5] revisited the idea considered in [4], by assuming that surface temperature and heat flux follow a power-law model. Vajravelu and Rollins [6] provided novel exact solutions for thermal transport in second grade fluid by incorporating heat dissipation terms in the model. Sadeghy et al. [7] put forward an excellent paper describing steady second grade fluid flow along a moving plate through numerical approach. Fluid motion affected by the presence of chemically reactive species in viscoelastic fluid was analyzed by Cortell [8] using numerical approach. Series solutions for second grade fluid flow triggered by an oscillatory deforming surface were furnished by Abbas et al. [9]. Sahoo [10] made use of an efficient numerical procedure to inspect third grade fluid flow by a radially deforming plate. Mishra et al. [11] also utilized second grade fluid model in order to analyze the flow of blood occurring in a channel with oscillatory expanding walls. A few noteworthy contributions in this dimension include the works of Turkyilmazoglu [12], Abbasbandy and Hayat [13], Sahoo and Poncet [14], Turkyilmazoglu [15]. Naganthran et al. [16], Mustafa [17] and Marinca and Marinca [18].

Boundary layer flow produced by a disk (infinitely large) revolving with uniform angular velocity in an otherwise stationary fluid was initially explored by von-Kármán [19]. Near the disk, purely circular motion is not possible due to lack of centrifugal force to accommodate radial pressure gradient. Consequently a radially outward flow is induced which in turn leads to a spiraling downward motion towards the disk. Later, Cochran [20] came up with an accurate power-series solution for the von-Kármán's system. Thermal transport in von-Kármán flow was addressed byMillsaps and Pohlhausen [21] for a variety of Prandtl numbers. Ackroyd [22] considered fluid flow produced by a permeable surface and provided novel series solutions involving exponential functions. The rotating-disk problem was attempted by Attia [23]for an

inelastic Reiner-Rivlin model. Takhar et al. [24] introduced unsteadiness in von-Karman flow by considering time dependent angular velocity of the rotating fluid. Ariel [25] examined the hydromagnetic flow along a rotating disk and derived computational results for wide range of magnetic interaction parameters. Miclavcic and Wang [26] extended the von-Kármán viscous pump problem by incorporating partial slip effects. They proved some existence and uniqueness results for the arising problem. An accurate power series solution for unsteady flow near a disk that undergoes uniform rotation from rest was provided by Xu and Liao [27]. Fang [28] analyzed von-Kármán model when the disk was allowed to stretch circumferentially. Some recent papers in the domain can be found through [29-43].

Many rotating disk systems including car breaking system, electrochemistry (rotating disk electrodes), chemical mixing chambers, geothermal extraction etc. involve viscoelastic liquids. Despite this fact, only a few articles describing von-Karman flow with viscoelastic fluids are published previously. Amongst these, Elliot [44] was perhaps the first to formulate rotating disk induced flow of Walters B fluid using standard boundary layer approximations. He noticed that elastic effects have a remarkable effect on the von-Karman's solution. Decades later, Ariel [45] made an attempt to model fluid flow above a rotating surface in second grade fluid. He was able to achieve self-similar velocity profiles by finite difference scheme. Perturbation solutions for small viscoelastic fluid parameter were also derived. In a latter paper [46], Ariel revisited this problem by adopting Walters-B model. Recently, Imtiaz et al. [47] considered fluid motion near a revolving disk of non-uniform thickness in MHD second grade fluid using homotopy approach.

In this thesis, firstly we endeavor to formulate second grade fluid flow triggered by a permeable rotating disk subjected to heat dissipation effects. This work also aims at deriving correct version of equations representing von-Kármán flow featuring second grade model. Secondly, we have noticed that the aforementioned publications do not address heat transfer problem in Von-Kármán flow involving Walters-B fluid. Thus our objective is to fill such gap and formulate energy equation in the existence of viscous dissipation effects.

1.8   Homotopy analysis method

Many real world problems are modeled using nonlinear differential equations and to determine exact solutions of these equations is usually not possible. So, we confine ourselves to approximation techniques in order to gain an insight into a particular nonlinear problem. In the

9

past, several attempts have been made in order to provide solution to these problems. One such mechanism was devised by Liao [48] named homotopy analysis method (HAM). Unlike previous perturbation techniques, this technique is valid even if there are no physical parameters in the problem. It is enriched with the convergence control parameter which can adjust and control the convergence region of the approximation series. This convergence control parameter can be optimized by minimizing the average squared residual of the governing equations in the frame of HAM in order to get a more accurate solution. To date a lot of improvements of HAM have been made in an attempt to make it valid for a bigger class of nonlinear equations.

Now, for a deeper understanding of the method, let us consider the classical Blasius equation with relevant boundary conditions:

$$F''' + \frac{1}{2} FF'' = 0, \tag{1.15a}$$

$$F(0) = 0, F'(0) = 0, F'(\infty) = 1, \tag{1.15b}$$

The first step in solving the problem using HAM is to construct the homotopy between linear and nonlinear operators using homotopy embedding parameter (also called zero-th order deformation equation).

Assume the embedding parameter $p \in [0,1]$ and $c_0 \neq 0$ denote the auxiliary parameter. The zero-th order deformation equation for the problem becomes

$$(1 - p)\mathcal{L}_F[F(\eta, p) - F_0(\eta)] = c_0 p N_F[F(\eta, p); \eta], \tag{1.16}$$

where $\mathcal{L}_F$ and N_F are auxiliary linear and nonlinear operators, $F_0(\eta)$ and $F(\eta, p)$ are defined as the initial approximation and unknown function respectively. The initial guess should be chosen so that it satisfies the initial and/or boundary conditions. The choice of linear operator and initial approximation greatly affects the form of solution. Let's set the initial approximation and auxiliary operator as

$$F_0(\eta) = \eta + \frac{e^{-3\eta} - 1}{3}; \mathcal{L}_F = \frac{\partial^3}{\partial \eta^3} + 3\frac{\partial^2}{\partial \eta^2}. \tag{1.17}$$

Clearly, at $p = 0$ and $p = 1$, one has

$$F(\eta, 0) = F_0(\eta), F(\eta, 1) = F(\eta). \tag{1.18}$$

Therefore, as p varies from 0 to 1, Eq. (1.16) varies continuously from initial guess to solution of non-linear equation Eq. (1.15a). The Taylor series expansion of unknown function $F(\eta, p)$ about $p = 0$ is given by:

$$F(\eta) = F_0(\eta) + \sum_{m=1}^{\infty} F_m(\eta); \quad F_m(\eta) = \frac{1}{m!} \frac{\partial^m F(\eta, p)}{\partial p^m}\bigg|_{p=0}. \tag{1.19}$$

The unknown terms of the series $F_m(\eta)$ can be worked out from mth order deformation equation which is obtained by differentiating the zero-th order deformation equation m times with respect to p, dividing by $m!$ and then substituting $p = 0$.

$$\mathcal{L}_F[F_m(\eta) - \chi_m F_{m-1}(\eta)] = c_0 R_{F,m}, \tag{1.20}$$

where χ_m and $R_{F,m}$ are defined as

$$\chi_m = \begin{cases} 0 & m \le 1 \\ 1 & m > 1 \end{cases}, \tag{1.21}$$

$$R_{F,m} = F'''_{m-1} + \frac{1}{2} \sum_{k=0}^{m-1} F_{m-1-k} F''_k. \tag{1.22}$$

It must be highlighted that, for $m \ge 1$, nonlinear problem gets replaced by linear sub problems which can then be solved easily using MATHEMATICA or MAPLE.
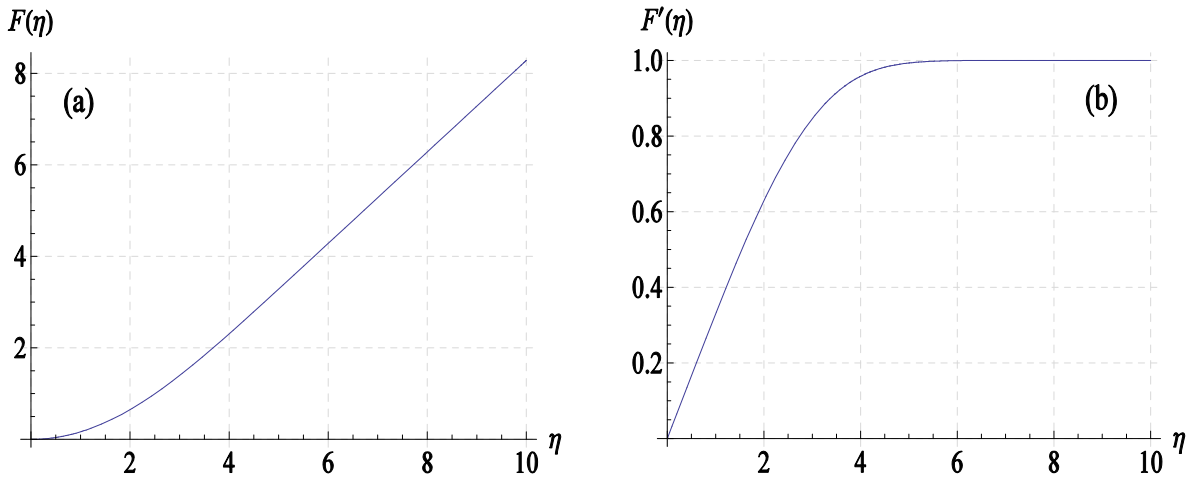
Fig. 1.2: Graphs of (a) F and (b) F' at 10th order of approximation.

Chapter 2

A novel formulation and analysis for transfer of heat in von-Kármán swirling flow involving viscoelastic fluid: OHAM solutions

In this chapter, consideration is given to the von-Kármán flow of viscoelastic fluid conforming with second grade model over a heated permeable disk. Our interest is to seek how fluid motion triggered around the disk is affected by the existence of both elasticity and viscous dissipation effects. It is found that the problem exhibits self-similar solution only when a prescribed wall temperature distribution is considered. Series solutions are worked out by using an easy to implement yet reliable routine BVPh 2.0 of MATHEMATICA based on the homotopy analysis method (HAM).

2.1 Mathematical Formulation

A laminar viscoelastic fluid flow triggered by uniform rotation of a large disk of radius R with constant angular speed ω is considered. Let (u, v, w) be the projections of velocity vector along radial, azimuthal and axial axes respectively, of cylindrical coordinate system (r, φ, z). Fluid flow is initiated due to uniform rotation of a relatively large disk about axial coordinate z. For simplicity, we suppose that disk is aligned with the plane $z = 0$ while fluid is equipped in semi-infinite region $z \geq 0$. Axial symmetry of the problem permits one to ignore variations of velocity in azimuthal directions. A uniform magnetic field of flux density B_0 is applied perpendicular to the flow direction. Accounting these assumptions, the relevant equations that describe the fluid flow above a rotating disk are:

$$\frac{\partial u}{\partial r} + \frac{u}{r} + \frac{\partial w}{\partial z} = 0, \tag{2.1}$$

$$\rho\left(u\frac{\partial u}{\partial r} + w\frac{\partial u}{\partial z} - \frac{v^2}{r}\right) = \frac{\partial \tau_{rr}}{\partial r} + \frac{\partial \tau_{rz}}{\partial z} + \frac{\tau_{rr} - \tau_{\varphi\varphi}}{r} - \sigma B_0^2 u, \tag{2.2}$$

$$\rho\left(u\frac{\partial v}{\partial r} + w\frac{\partial v}{\partial z} + \frac{uv}{r}\right) = \frac{\partial \tau_{r\varphi}}{\partial r} + \frac{\partial \tau_{z\varphi}}{\partial z} + \frac{2\tau_{r\varphi}}{r} - \sigma B_0^2 v, \tag{2.3}$$

$$\rho\left(u\frac{\partial w}{\partial r} + w\frac{\partial w}{\partial z}\right) = \frac{\partial \tau_{rz}}{\partial r} + \frac{\partial \tau_{zz}}{\partial z} + \frac{\tau_{rz}}{r}, \tag{2.4}$$

where τ_{ij} $(i,j = 1 - 3)$ are components of stress tensor $\boldsymbol{\tau}$ proposed by Rivlin and Ericksen for viscoelastic fluids (see chapter 1 for details).

The components of the stress tensor $\boldsymbol{\tau}$ in cylindrical coordinates are obtained as follows:

$$\tau_{rr} = -p + 2\mu\frac{\partial u}{\partial r} + 2\alpha_1\left\{u\frac{\partial^2 u}{\partial r^2} + w\frac{\partial^2 u}{\partial r\partial z} + 2\left(\frac{\partial u}{\partial r}\right)^2 + \left(\frac{\partial v}{\partial r} - \frac{v}{r}\right)^2 + \frac{\partial w}{\partial r}\left(\frac{\partial u}{\partial z} + \frac{\partial w}{\partial r}\right)\right\}$$
$$+ \alpha_2\left\{4\left(\frac{\partial u}{\partial r}\right)^2 + \left(\frac{\partial v}{\partial r} - \frac{v}{r}\right)^2 + \left(\frac{\partial u}{\partial z} + \frac{\partial w}{\partial r}\right)^2\right\}, \tag{2.5}$$

$$\tau_{\varphi\varphi} = -p + 2\mu\frac{u}{r} + 2\alpha_1\left\{\frac{u}{r}\frac{\partial u}{\partial r} + \frac{u^2}{r^2} + \frac{w}{r}\frac{\partial u}{\partial z} + \frac{u^2}{r^2}\right\} + \alpha_2\left\{4\left(\frac{u}{r}\right)^2 + \left(\frac{\partial v}{\partial r} - \frac{v}{r}\right)^2 + \left(\frac{\partial v}{\partial z}\right)^2\right\}, \tag{2.6}$$

$$\tau_{zz} = -p + 2\mu\frac{\partial w}{\partial z} + 2\alpha_1\left\{u\frac{\partial^2 w}{\partial r\partial z} + w\frac{\partial^2 w}{\partial z^2} + \frac{\partial u}{\partial z}\left(\frac{\partial u}{\partial z} + \frac{\partial w}{\partial r}\right) + \left(\frac{\partial v}{\partial z}\right)^2 + 2\left(\frac{\partial w}{\partial z}\right)^2\right\}$$
$$+ \alpha_2\left\{\left(\frac{\partial u}{\partial z} + \frac{\partial w}{\partial r}\right)^2 + \left(\frac{\partial v}{\partial z}\right)^2 + 4\left(\frac{\partial w}{\partial z}\right)^2\right\}, \tag{2.7}$$

$$\tau_{r\varphi} = \mu\left(\frac{\partial v}{\partial r} - \frac{v}{r}\right) + \alpha_1\left\{u\frac{\partial^2 v}{\partial r^2} + \left(\frac{\partial u}{\partial r} + 2\frac{u}{r} + w\frac{\partial}{\partial z}\right)\left(\frac{\partial v}{\partial r} - \frac{v}{r}\right) + \frac{\partial v}{\partial z}\frac{\partial w}{\partial r}\right\}$$
$$+ \alpha_2\left\{2\left(\frac{\partial u}{\partial r} + \frac{u}{r}\right)\left(\frac{\partial v}{\partial r} - \frac{v}{r}\right) + \frac{\partial v}{\partial z}\left(\frac{\partial u}{\partial z} + \frac{\partial w}{\partial r}\right)\right\}, \tag{2.8}$$

$$\tau_{\varphi z} = \mu\frac{\partial v}{\partial z} + \alpha_1\left\{u\frac{\partial^2 v}{\partial r\partial z} + w\frac{\partial^2 v}{\partial z^2} + \frac{\partial u}{\partial z}\left(\frac{\partial v}{\partial r} - \frac{v}{r}\right) + 3\frac{u}{r}\frac{\partial v}{\partial z} + \frac{\partial v}{\partial z}\frac{\partial w}{\partial z}\right\}$$
$$+ \alpha_2\left\{\left(\frac{\partial u}{\partial z} + \frac{\partial w}{\partial r}\right)\left(\frac{\partial v}{\partial r} - \frac{v}{r}\right) + 2\frac{u}{r}\frac{\partial v}{\partial z} + 2\frac{\partial v}{\partial z}\frac{\partial w}{\partial z}\right\}, \tag{2.9}$$

$$\tau_{rz} = \mu\left(\frac{\partial u}{\partial z} + \frac{\partial w}{\partial r}\right)$$
$$+ \alpha_1\left\{\left(u\frac{\partial}{\partial r} + w\frac{\partial}{\partial z}\right)\left(\frac{\partial u}{\partial z} + \frac{\partial w}{\partial r}\right) + 2\frac{\partial v}{\partial z}\left(\frac{\partial v}{\partial r} - \frac{v}{r}\right) + \frac{\partial u}{\partial r}\frac{\partial w}{\partial r} + \frac{\partial u}{\partial z}\frac{\partial w}{\partial z}\right.$$
$$\left. + 3\left(\frac{\partial u}{\partial r}\frac{\partial u}{\partial z} + \frac{\partial w}{\partial z}\frac{\partial w}{\partial r}\right)\right\} + \alpha_2\left\{2\left(\frac{\partial u}{\partial r} + \frac{\partial w}{\partial z}\right)\left(\frac{\partial u}{\partial z} + \frac{\partial w}{\partial r}\right) + \frac{\partial v}{\partial z}\left(\frac{\partial v}{\partial r} - \frac{v}{r}\right)\right\}. \tag{2.10}$$

By making use of Eqs. (2.5)-(2.10) and the boundary layer approximations, Eqs. (2.2) and (2.3) take the form

$$u\frac{\partial u}{\partial r} + w\frac{\partial u}{\partial z} - \frac{v^2}{r} = \nu\frac{\partial^2 u}{\partial z^2} + \frac{\alpha_1}{\rho}\left\{\begin{array}{l} u\dfrac{\partial^3 u}{\partial r\partial z^2} + w\dfrac{\partial^3 u}{\partial z^3} + \dfrac{\partial u}{\partial r}\dfrac{\partial^2 u}{\partial z^2} - \dfrac{\partial u}{\partial z}\dfrac{\partial^2 w}{\partial z^2} \\ + \dfrac{\partial^2 v}{\partial z^2}\left(\dfrac{\partial v}{\partial r} - \dfrac{v}{r}\right) + \dfrac{\partial v}{\partial z}\dfrac{\partial^2 v}{\partial r\partial z} - \dfrac{1}{r}\left(\dfrac{\partial u}{\partial z}\right)^2 \end{array}\right\} - \frac{\sigma B_0^2}{\rho}u, \tag{2.11}$$

$$u\frac{\partial v}{\partial r} + w\frac{\partial v}{\partial z} + \frac{uv}{r} = v\frac{\partial^2 v}{\partial z^2} + \frac{\alpha_1}{\rho}\left\{ \begin{array}{c} -\dfrac{\partial v}{\partial z}\dfrac{\partial^2 u}{\partial r\partial z} + u\dfrac{\partial^3 v}{\partial r\partial z^2} + w\dfrac{\partial^3 v}{\partial z^3} + \dfrac{u}{r}\dfrac{\partial^2 v}{\partial z^2} \\ -\dfrac{\partial v}{\partial z}\dfrac{\partial^2 w}{\partial z^2} - \dfrac{1}{r}\dfrac{\partial u}{\partial z}\dfrac{\partial v}{\partial z} \end{array} \right\} - \frac{\sigma B_0^2}{\rho}v, \qquad (2.12)$$

where σ shows fluid electrical conductivity, ρ is termed as density, v stands for kinematic viscosity coefficient and $\alpha_1 > 0$ is the material constant which accounts for viscoelasticity of the fluid.

Since the surface is permeable and exhibits no slip, one can write

$$z = 0: \quad u = 0, \quad v = r\omega, \quad w = -w_0. \qquad (2.13)$$

And since the lateral velocities vanish far above the disk, one can express

$$z \to \infty: \quad u \to 0, \quad v \to 0. \qquad (2.14)$$

We express the velocities (u, v, w) as follows:

$$u = r\omega F'(\eta), \quad v = r\omega G(\eta), \quad w = -2\sqrt{\omega v}F(\eta), \qquad (2.15)$$

where $\eta = z\,(\omega/v)^{1/2}$ is the dimensionless axial distance whereas the terms $\sqrt{\omega/v}$ and $\sqrt{\omega v}$ are characteristic length and velocity scales of the problem.

Note that variables introduced in Eq. (2.15) satisfy Eq. (2.1), whereas Eqs. (2.11) and (2.12) change into the following ODEs:

$$F''' + G^2 + 2FF'' - F'^2 + K\big(2F'F''' + F''^2 + G'^2 - 2FF''''\big) - MF' = 0, \qquad (2.16)$$

$$G'' - 2F'G + 2FG' + K(-2FG''' + 2F'G'') - MG = 0, \qquad (2.17)$$

and the boundary conditions take the form:

$$F(0) = S, \quad F'(0) = 0, \quad G(0) = 1, \qquad (2.18a)$$

$$F' \to 0, \quad G \to 0 \text{ as } \eta \to \infty, \qquad (2.18b)$$

where $S = w_0/2\sqrt{\omega v}$ is the wall suction parameter, $K = \alpha_1\omega/\mu$ is the viscoelastic fluid parameter and $M = \sigma B_0^2/\rho\omega$ is the magnetic interaction parameter.

2.2 Heat transfer analysis

Following Vajravelu and Rollins [6], heating process of the disk is characterized by a quadratic temperature distribution $T_w = T_\infty + br^2$ where b is a constant with dimension $\{\Theta L^{-2}\}$ and T_∞ symbolizes ambient fluid temperature.Accounting viscous dissipation effect, the energy equation is given below:

$$\rho C_p \left(u \frac{\partial T}{\partial r} + w \frac{\partial T}{\partial z} \right) = \kappa \left\{ \frac{1}{r} \frac{\partial}{\partial r} \left(r \frac{\partial T}{\partial r} \right) + \frac{\partial^2 T}{\partial z^2} \right\} + \Phi, \tag{2.19}$$

where C_p denotes specific heat capacity, κ represents the thermal conductivity of fluid and Φ is dissipation function which is defined as:

$$\Phi = \tau_{rr} \left(\frac{\partial u}{\partial r} \right) + \tau_{\varphi\varphi} \left(\frac{u}{r} \right) + \tau_{zz} \left(\frac{\partial w}{\partial z} \right) + \tau_{r\varphi} \left(\frac{\partial v}{\partial r} - \frac{v}{r} \right) + \tau_{\varphi z} \left(\frac{\partial v}{\partial z} \right) + \tau_{rz} \left(\frac{\partial u}{\partial z} + \frac{\partial w}{\partial r} \right), \tag{2.20}$$

in which components of stress tensor satisfy the second grade model. Eq. (2.19) via boundary layer approximations is given below:

$$u \frac{\partial T}{\partial r} + w \frac{\partial T}{\partial z} = \frac{\kappa}{\rho C_p} \frac{\partial^2 T}{\partial z^2} + \frac{\alpha_1}{\rho C_p} \left\{ u \frac{\partial u}{\partial z} \frac{\partial^2 u}{\partial r \partial z} + w \frac{\partial u}{\partial z} \frac{\partial^2 u}{\partial z^2} + u \frac{\partial v}{\partial z} \frac{\partial^2 v}{\partial r \partial z} + w \frac{\partial v}{\partial z} \frac{\partial^2 v}{\partial z^2} \right\}$$
$$+ \frac{\mu}{\rho C_p} \left\{ \left(\frac{\partial u}{\partial z} \right)^2 + \left(\frac{\partial v}{\partial z} \right)^2 \right\}. \tag{2.21}$$

Defining the non-dimensional temperature as $\theta(\eta) = (T - T_\infty)/(T_w - T_\infty)$, Eq. (2.21) takes the form:

$$\frac{1}{Pr} \theta'' - 2F'\theta + 2F\theta' + Ec\left(F''^2 + G'^2\right) + KEc\{F'\left(F''^2 + G'^2\right) - 2F(F''F''' + G'G'')\} = 0, \tag{2.22}$$

Eq. (2.22) is to be solved for

$$\theta(0) = 1 \text{ and } \theta \to 0 \text{ as } \eta \to \infty, \tag{2.23}$$

where $Pr = \mu C_p / \kappa$ defines the Prandtl number and $Ec = \omega^2 / C_p b$ gives the Eckert number. Note that only present choice of quadratic surface temperature yields a constant Eckert number or equivalently self-similar equation (2.22). We therefore remark that only a locally similar solution would be possible in case of constant wall temperature.

Governing system posed by (2.16)-(2.18b), (2.22) and (2.23) collapses to the Newtonian fluid case when $K = 0$ whereas the case $Ec = 0$ corresponds to the situation where heat dissipation effects are absent. Furthermore, the cases of hydrodynamic flow and impermeable surface are recovered when $M = 0$ and $S = 0$ respectively.

After finding mean flow quantities, our main interest lies in determining the drag coefficient, resisting torque, wall heat transfer rate and volumetric flow rate since these are the most important tools from engineering point of view. Skin friction coefficient in radial direction is defined below:

$$C_{f_r} = \frac{\tau_{zr}|_{z=0}}{\rho r^2 \omega^2},$$

(2.24)

where radial stress τ_{rz} is given by:

$$\tau_{zr} = \mu \frac{\partial u}{\partial z} + \alpha_1 \left\{ u \frac{\partial^2 u}{\partial r \partial z} + w \frac{\partial^2 u}{\partial z^2} + \frac{\partial u}{\partial r} \frac{\partial u}{\partial z} - \frac{\partial u}{\partial z} \frac{\partial w}{\partial z} + \frac{\partial v}{\partial z} \left(\frac{\partial v}{\partial r} - \frac{v}{r} \right) \right\},$$

(2.25)

By making use of Eq. (2.15), we arrive at

$$\sqrt{Re_r} C_{f_r} = F''(0) - 2KF(0)F'''(0),$$

(2.26)

Another notable quantity is moment coefficient defined below (see Attia [29]):

$$C_{m,r} = \frac{T_r}{\rho \omega^2 r^5},$$

(2.27)

where the torque required T_r is evaluated as follows:

$$T_r = \int_0^r \tau_{z\theta}|_{z=0} 2\pi r^2 dr,$$

(2.28)

in which azimuthal stress $\tau_{z\theta}$ is obtained as:

$$\tau_{z\theta} = \mu \frac{\partial v}{\partial z} + \alpha_1 \left\{ u \frac{\partial^2 v}{\partial r \partial z} + w \frac{\partial^2 v}{\partial z^2} + \frac{u}{r} \frac{\partial v}{\partial z} - \frac{\partial v}{\partial z} \frac{\partial w}{\partial z} \right\}.$$

(2.29)

Invoking transformations (2.15), we arrive at the following:

$$C_{m,r} = \frac{\pi}{2} \frac{1}{\sqrt{Re_r}} \left(G'(0) - 2KF(0)G''(0) \right).$$

(2.30)

Defining the Nusselt number as $Nu = -Lk(\partial T/\partial z)_{z=0}/(T_w - T_\infty)$ [38] with $L = \sqrt{v/\omega}$ as the characteristic length scale, we obtain the following

$$Nu = -\theta'(0).$$

(2.31)

Since the disk draws fluid in the vertical direction at the rate $w(\infty)$ so finite disk's pumping efficiency with radius R can be worked out via given definite integral:

$$Q = \int_0^R -w(\infty) 2\pi r dr = 2\sqrt{v\omega} F(\infty) \pi R^2.$$

(2.32)

The set of equations (2.27)-(2.30) clearly suggest that one has to closely analyze the variation of $F''(0), G'(0), \theta'(0)$ and $F(\infty)$ to discover the physical features of the considered problem.

16

2.3 Series solution

The governing problem constitutes a coupled system of nonlinear ordinary differential equations with apparently no exact solution. Hence we look for approximate (analytical) solution by making use of an easy-to-implement MATHEMATICA package called BVPh2.0 which is based on homotopy analysis method. This package can treat a variety of coupled non-linear problems with finite and infinite domains. In BVPh 2.0, one needs to write the governing equations along with the boundary conditions, initial approximations of the unknown functions and linear operators corresponding to each equation.

Homotopy analysis technique uses a concept from topology to transfer a non-linear problem into an infinite set of linear sub-problems. Following Liao [48], we consider series solutions of Eqs. (2.16), (2.17) and (2.22) subject to conditions (2.18a), (2.18b) and (2.23) in the forms:

$$F(\eta) = \sum_{k=0}^{+\infty} F_k(\eta), \ \ G(\eta) = \sum_{k=0}^{+\infty} G_k(\eta), \ \ \theta(\eta) = \sum_{k=0}^{+\infty} \theta_k(\eta), \tag{2.33}$$

where F_k, G_k and θ_k for $k \geq 1$ are worked out from the so-called k^{th}−order deformation equations associated with the current problem. Following Liao [27] we assume the base functions to be of the type $\{\eta^m e^{-n\eta} \mid m \geq 0, n \geq 0\}$. Keeping in view the boundary conditions, following initial approximations are opted:

$$F_0(\eta) = S, \ \ G_0(\eta) = e^{-\eta}, \ \ \theta_0(\eta) = e^{-\eta}, \tag{2.34}$$

And the auxiliary linear operators $\mathcal{L}_F, \mathcal{L}_G, \mathcal{L}_\theta$ for the system are chosen as:

$$\mathcal{L}_F \equiv \frac{\partial^3}{\partial \eta^3} - \frac{\partial}{\partial \eta}, \ \mathcal{L}_G \equiv \frac{\partial^2}{\partial \eta^2} - 1, \ \mathcal{L}_\theta \equiv \frac{\partial^2}{\partial \eta^2} - 1, \tag{2.35}$$

It should be noted that operators defined above exhibit the properties:

$$\mathcal{L}_F[c_1 + c_2 e^{-\eta} + c_3 e^{\eta}] = 0, \tag{2.36}$$

$$\mathcal{L}_G[c_4 e^{-\eta} + c_5 e^{\eta}] = 0, \tag{2.37}$$

$$\mathcal{L}_\theta[c_6 e^{-\eta} + c_7 e^{\eta}] = 0, \tag{2.38}$$

where $c_i (i = 1 - 7)$ are unknown constants to find out.

It should be remarked here that the functions F, G and θ obtained via BVPh 2.0 contain auxiliary parameters c_0^F, c_0^G and c_0^θ which have essential role in establishing the convergence of series solutions. The procedure of finding these auxiliary parameters is described in several papers

including [48]. Here we are interested to find *optimal* values of such parameters (which gives the lowest averaged squared residual), as done in many previous works including refs. [49]-[52].

The total averaged squared residual $E_{T,k}$ is defined as follows:

$$E_{T,k} = E_{F,k} + E_{G,k} + E_{\theta,k}, \tag{2.39}$$

where $E_{F,k}$, $E_{G,k}$ and $E_{\theta,k}$ are average squared residuals of equations (2.16), (2.17) and (2.22) defined as:

$$E_{F,k} = \frac{1}{b-a} \int_a^b (\mathcal{N}_F[F_k(\eta), G_k(\eta)])^2 \, d\eta, \tag{2.40}$$

$$E_{G,k} = \frac{1}{b-a} \int_a^b (\mathcal{N}_G[F_k(\eta), G_k(\eta)])^2 \, d\eta, \tag{2.41}$$

$$E_{\theta,k} = \frac{1}{b-a} \int_a^b (\mathcal{N}_\theta[F_k(\eta), G_k(\eta), \theta_k(\eta)])^2 \, d\eta, \tag{2.42}$$

in which $\mathcal{N}_F$, $\mathcal{N}_G$ and $\mathcal{N}_\theta$ are the associated non-linear operators. The optimal values of c_0^F, c_0^G and c_0^θ, corresponding to the minimum value of Eq. (2.39), can be retrieved by command "GetOptiVar" of BVPh 2.0.For details, the reader is referred to the user's guide available online (http://numericaltank.sjtu.edu.cn/BVPh.htm)

2.4 Results and discussion

The approach explained above has been utilized to obtain series solutions for diverse range of controlling parameters. Fig. 2.1 plots the total averaged squared residual $E_{T,k}$ versus the order of approximations. It can clearly be seen that total error in the system is drastically reduced as we increase the order of approximation which guarantees the convergence. Figs. 2.2a-2.2d show evolution of velocity components and temperature for values of viscoelastic fluid parameter K up to 1.6. The presented results correspond to 20th order HAM solutions. Axial velocity profile represented by $F(\eta)$ is seen to enhance as K enlarges. Fig. 2.2b shows that radial velocity, proportional to $F'(\eta)$, grows upon increasing K. It means that radially outward flow triggered by disk centrifugal effect accelerates for increasing values of K. Circumferential motion is much enhanced due to the inclusion of elasticity effects. These outcomes are of no surprise since elastic forces act as tensile stresses which tend to accelerate the fluid flow. Figs. 2.2a-2.2c clarify that, as K enlarges, the boundary layer expands greatly and reaches a constant value as K tends to infinity ($K \to \infty$).Similar to the velocity profiles, temperature θ is also proportional to the

parameter K. It can therefore be inferred that elasticity effects combined with viscous dissipation elevates thermal boundary layer.

To examine the behavior that wall permeability can have on the flow model, we computed solution profiles for a variety of wall suction parameters in Figs. 2.3a-2.3d. In line with the previous works (see [41] and articles there in.), axial flow attains a constant velocity for sufficiently large values of S. Naturally, axial flow is expected to accelerate upon increasing suction velocity (see Fig. 2.3a). The enhanced wall suction opposes the radially outward flow generated by disk centrifugal effect. Therefore, radial velocity profile (related with $F'(\eta)$) is seen to reduce as S enlarges. Suction effect also provides resistance to the circular motion as apparent from Fig. 2.3c. Moreover, Fig. 2.3d shows an expansion in thermal boundary layer for increasing S. Physically, the volume of (cold) fluid being entrained is predicted to rise in the existence of suction. Due to this reason, one expects temperature profile to become broader whenever S is incremented.

To analyze how present flow model is affected by the action of transverse magnetic field, we prepared Figs. 2.4a-2.4d which display variations in the solutions with vertical distance for a variety of magnetic interaction parameters. Under magnetic field, boundary layer is substantially thinned compared with the case of no magnetic field. Axially downward flow is naturally opposed by the Lorentz force induced by magnetic field vertically upward (see Fig. 2.4a). Both radial and circular flows also slow down due to the presence of Lorentz force. Note that the deceleration in entrained flow caused by increasing Lorentz force reduces the volume of ambient (cold) fluid sucked towards disk, thereby increasing thermal penetration depth.

To visualize the consequences of viscous dissipation on the flow model, we compute temperature curves at different values of Prandtl number Pr and Eckert number Ec in Figs. 2.5a and 2.5b respectively. It is apparent the temperature curves become less steep for lower Prandtl number suggesting that $\theta'(0)$ vanishes when $Pr \rightarrow 0$. Increase in Eckert number may be attributed to the growth in fluid average kinetic energy or reduction in its enthalpy difference. In other words, Eckert number characterizes self-heating of fluid caused by dissipation effects. Therefore, temperature distribution erupts for increasing Eckert number Ec values.

Figs. 2.6a-2.6d portray the variations in skin friction coefficients, Nusselt number and entrainment velocity with viscoelastic parameter K for a variety of magnetic interaction

parameters. The results predict that overall drag experienced at the surface would increase due to inclusion of elasticity effects. Also, heat transfer rate determined by Nusselt number elevates as K becomes large. Entrainment velocity measuring the disk pumping efficiency is accelerated when higher values of K are employed.

Table 2.1 shows that present results are in perfect agreement with numerical solutions furnished by Ariel [25]. Tables 2.2 and 2.3 include the computational results for skin friction coefficients, Nusselt number and velocity of entrained fluid for varying choices of parameters. Naturally, the effect of wall suction is to promote the axial flow at the far field. As a consequence, a marked rise in drag force is noted for increasing values of S. The transfer of heat from solid surface is appreciably elevated due to consideration of wall suction. However, it is much lowered whenever heat dissipation effects are present.
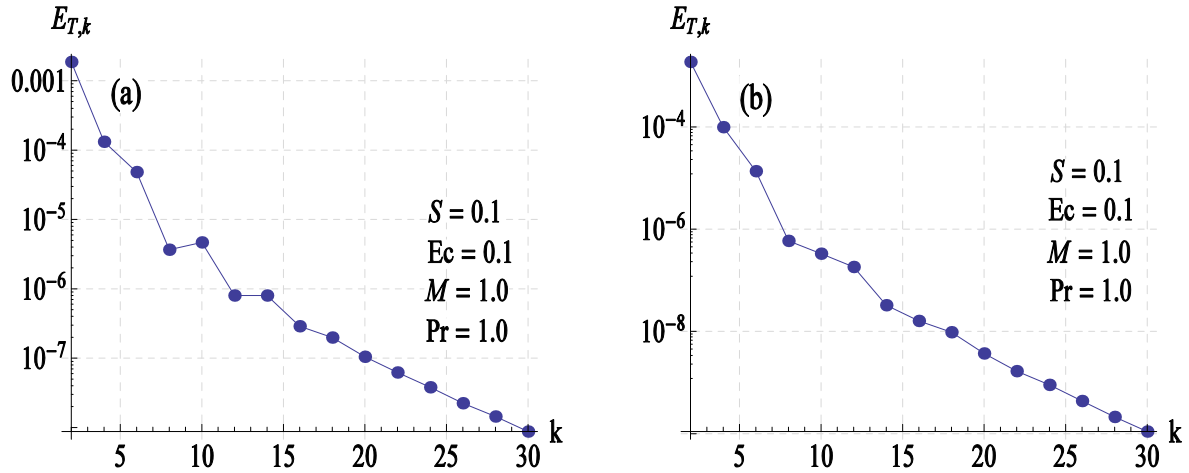
Fig. 2.1: Variation in averaged squared residual $E_{T,k}$ with order of approximations k(a) $K = 0$ and (b)$K = 0.5$.
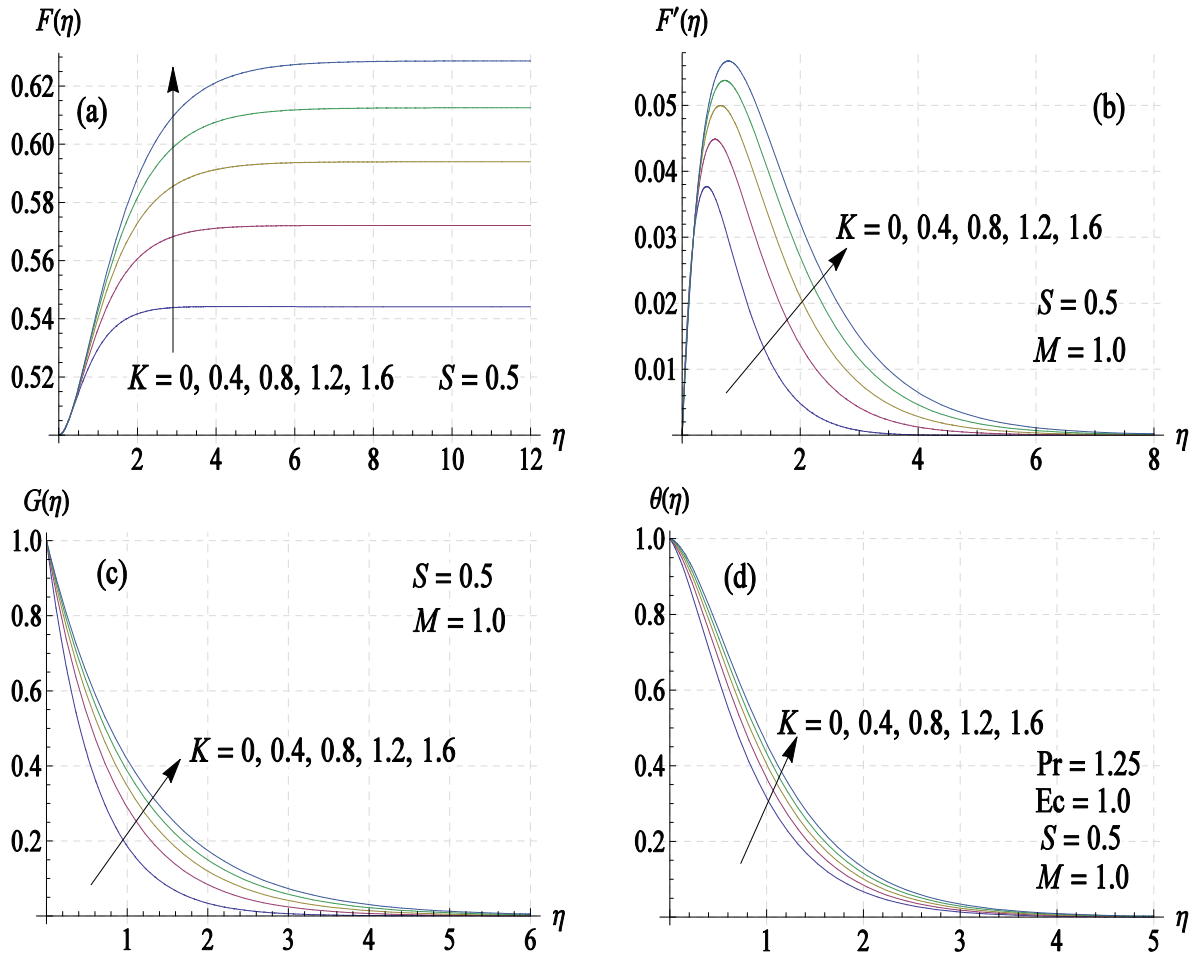
Fig. 2.2: Change in velocities (F, F', G) and temperature (θ) against η for varying choices of viscoelastic fluid parameter K.
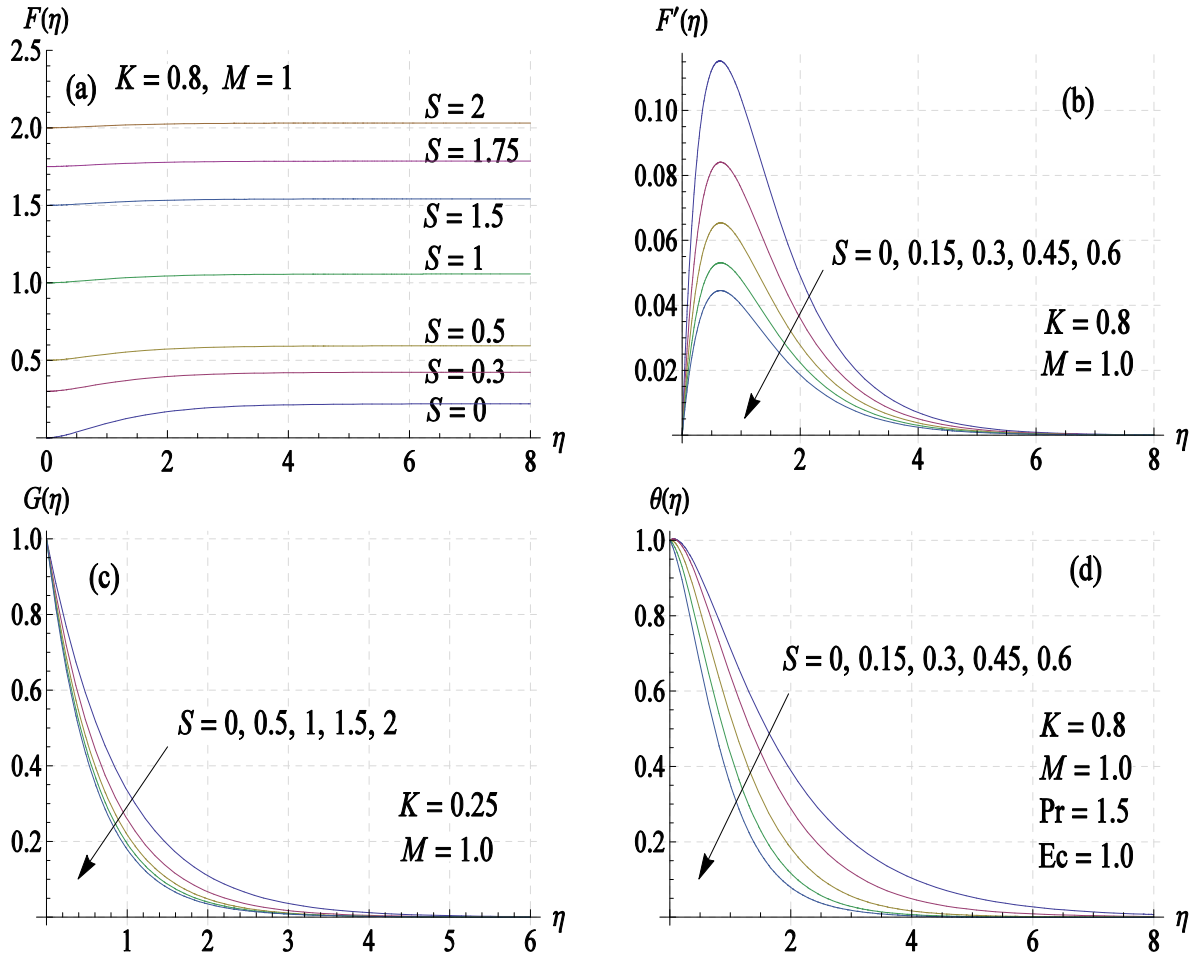
Fig. 2.3: Change in components of velocity (F, F', G) and temperature (θ) against η for varying choices of wall suction parameter S.
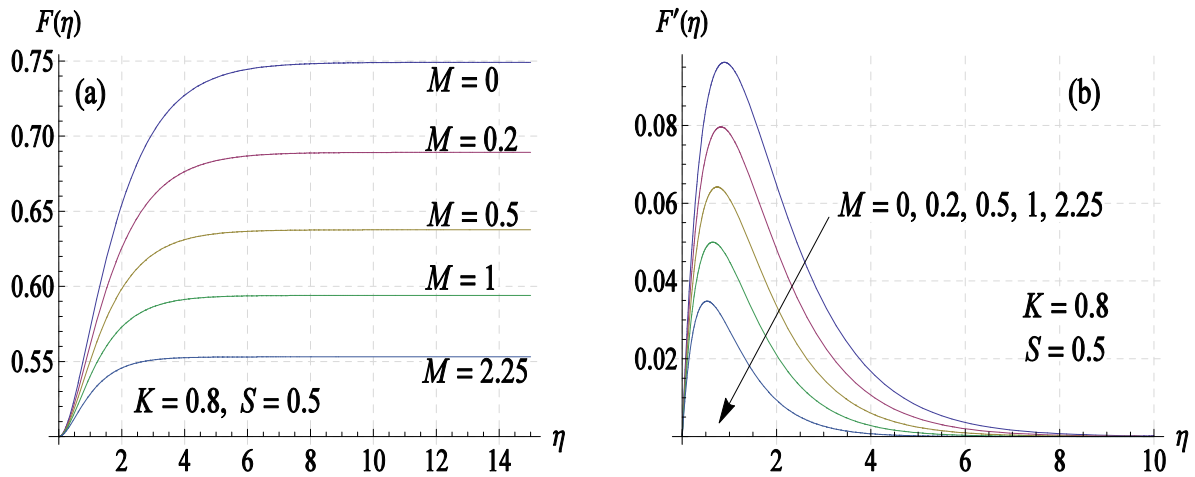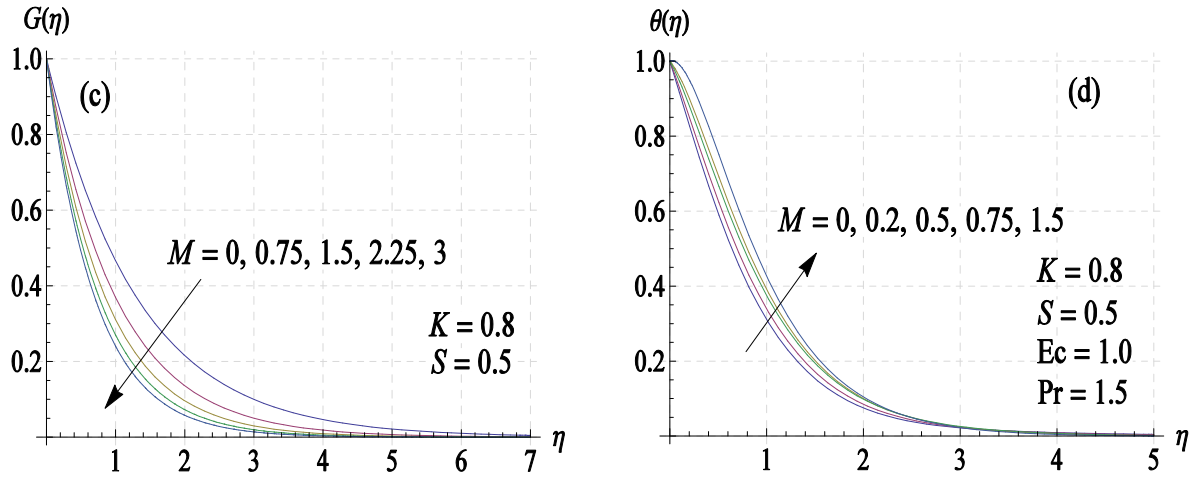
Fig. 2.4: Change in velocities (F, F', G) and temperature (θ) for a varying choices of magnetic interaction parameter M.
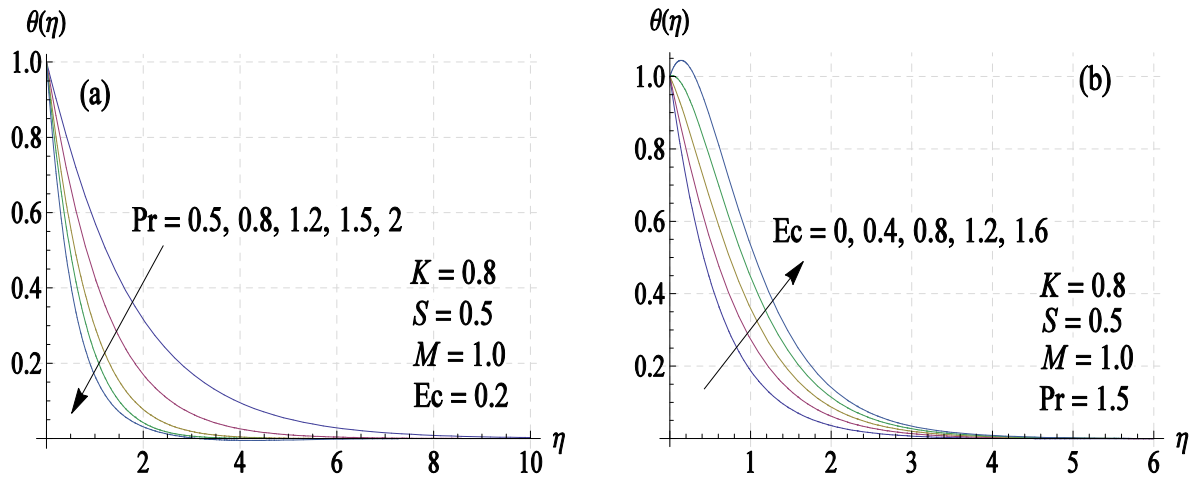
Fig. 2.5: Change in fluid temperature against vertical distance η for varying choices of (a) Prandtl number Pr and (b) Eckert number Ec.
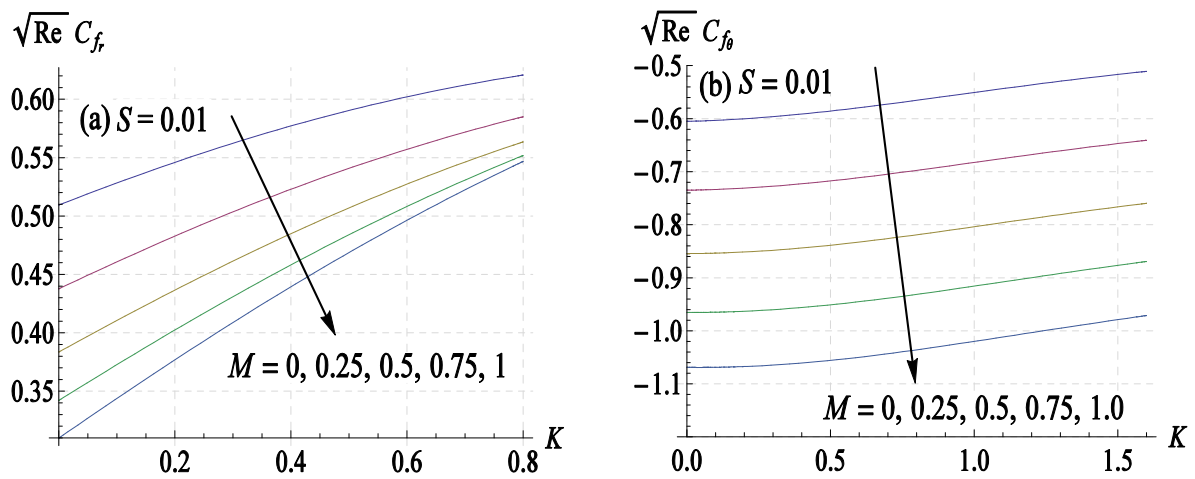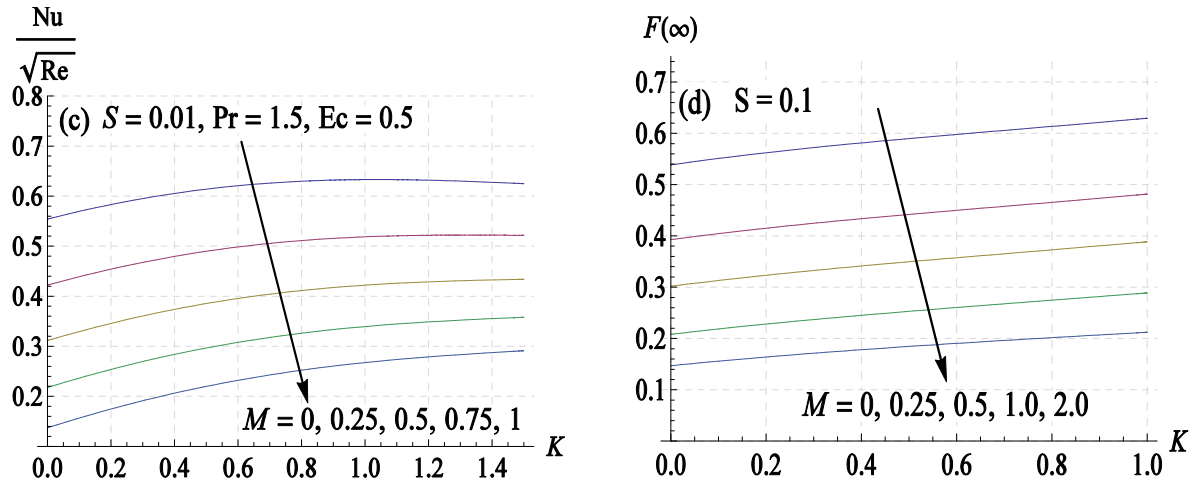
Fig. 2.6: Profiles of skin-friction coefficients, Nusselt number and volume flow rate versus viscoelastic fluid parameter K for varying choices of M.

Table 2.1: A comparison of 45th order HAM results with those obtained by Ariel [25] for different values of M when $K = S = 0$.

M	$F''(0)^a$	$-G'(0)^a$	$F''(0)^b$	$-G'(0)^b$
0.2	0.453141	0.708795	0.453129	0.708793
0.4	0.405576	0.802376	0.405576	0.802376
0.6	0.366698	0.894476	0.366698	0.894476
0.8	0.335092	0.983607	0.335090	0.983607
1.0	0.309258	1.069053	0.309258	1.069053
1.2	0.287915	1.150635	0.287915	1.150635
1.4	0.270049	1.228466	0.270049	1.228466
1.6	0.254892	1.302793	0.254892	1.302793
2.0	0.230559	1.442094	0.230559	1.442094

[a] Denotes results obtained by Ariel [25].
[b] Denotes results of current study.

Table 2.2: Computational results of skin-friction coefficients for varying choices of K, M and S at 20th-order of approximations.

K	S	M	$F(\infty)$	$Re^{\frac{1}{2}}C_{f_r}$	$Re^{\frac{1}{2}}C_{f_\theta}$
0	0.5	1	0.54552	0.25104	-1.65707
0.25			0.56299	0.46619	-1.79271
0.5			0.57776	0.62410	-1.87536
1			0.63375	0.86356	-2.00000
0.5	0		0.18737	0.46387	-1.04564

Table 2.2 *(continued)*

K	S	M	$F(\infty)$	$Re^{\frac{1}{2}}C_{f_r}$	$Re^{\frac{1}{2}}C_{f_\theta}$
	0.15		0.28867	0.54084	-1.27874
	0.3		0.40615	0.58866	-1.52255
	0.5		0.57776	0.62410	-1.87536
	0.5	0	0.70561	0.73155	-1.17555
		0.4	0.62815	0.66475	-1.48226
		1	0.57776	0.62410	-1.87536
		2.5	0.53986	0.60114	-2.64959

Table 2.3: Computational results of Nusselt number for varying choices of K, M and S at 20th-order of approximations.

K	S	M	Pr	Ec	$-\theta'(0)$
0	0.5	1	1.25	0.5	0.82610
0.4					0.78676
0.8					0.76409
1.5					0.72844
0.5	0				0.19961
	0.4				0.62337
	0.8				1.29921
	1				1.66176
	0.5	0			1.07810
		0.3			0.97080
		0.6			0.88221
		1			0.78016
		1	0.5		0.34936
			0.8		0.52575
			1.25		0.78016
			1.75		1.05578
			1.25	0	1.36207
				0.4	0.89690
				0.8	0.42966
				1.25	-0.09439

2.5 Concluding remarks

Self-similar solutions are determined for the transfer of heat in von-Kármán flow (of infinite disk) involving second grade fluid. The disk is assumed permeable with a prescribed (quadratic) temperature distribution $T_w(r)$. A reliable package BVPh 2.0 based on homotopy analysis method is applied to determine velocity and temperature fields. Important outcomes of this research are outlined below:

- Our computations reflect an almost linear decrease in total squared residual with increasing order of approximations. At 30th –order approximation, total squared residual is found to be 10^{-8} which validates the employed method.

- In line with [7], influence of fluid's elasticity is to enhance boundary layer thicknesses as well as shear stresses experienced at the wall. The volume of fluid entrained (at the disk) is also enhanced when elastic effects are accounted.

- Notably, circumferential wall shear is inversely proportional to K in case of impermeable surface.

- Wall permeability gives opposition to both outwardly directed radial flow generated by disk centrifugal effect as well as circumferential flow induced by disk rotation.

- Naturally, the action of wall suction accelerates the entrained flow and elevates resisting wall shear.

- When viscous dissipation is negligible, temperature profile moves closer to the wall as K enlarges, illustrating a reduction in thermal penetration depth. Intriguingly, an opposite trend is noticed when viscous dissipation term is retained. Though the variation in θ with K is only marginal.

- The Nusselt number increases in absolute sense when elastic effects are incorporated in the problem.

Chapter 3

A study of elastico-viscous fluid flow by a revolving disk with heat dissipation effects using HAM based package BVPh 2.0

Von-Kármán problem of infinite disk is re-examined when fluid under consideration is elastico-viscous, satisfying the constitutive relations of Walters-B model. Main target here is to demonstrate how the presence of elasticity alters heat transfer phenomenon for the said problem especially when heat dissipation term is included in the analysis. We assume a self-similarity solution that results in a system of coupled nonlinear differential equations. An easy to use package BVPh 2.0 based on the homotopy analysis method (HAM) is used to present series solutions for values of elastic-viscous fluid parameter (K) in the range $0 \leq K \leq 1$.

3.1   Problem formulation

Suppose that an electrically conducting elastico-viscous fluid flows due to steady rotation of an infinite plane surface. Fluid is exposed to axial magnetic field with uniform magnetic flux density B_0. In a cylindrical coordinate system (r, φ, z), the disk taken along $z = 0$ is made to rotate steadily about the axis $r = 0$. Fluid motion takes place in the semi-infinite region $z \geq 0$ and $z = 0$ is the only boundary. Let u, v and w symbolize velocity vector projections along $r-, \varphi-$ and $z-$ directions respectively. Assuming that electric field is absent and magnetic Reynolds number is small enough so that induced magnetic field is negligible, components of Lorentz force vector are $F_r = -\sigma B_0^2 u$, $F_\varphi = -\sigma B_0^2 v$ and $F_z = 0$, where σ is the fluid electrical conductivity. Since the problem is symmetric about the vertical axis, one can neglect variation in velocities in φ-direction, that is, $\partial/\partial\varphi \equiv 0$. Relevant equations embodying fluid flow about a rotating disk are:

$$\frac{\partial u}{\partial r} + \frac{u}{r} + \frac{\partial w}{\partial z} = 0, \tag{3.1}$$

$$\rho\left(u\frac{\partial u}{\partial r} + w\frac{\partial u}{\partial z} - \frac{v^2}{r}\right) = \frac{\partial \tau_{rr}}{\partial r} + \frac{\partial \tau_{rz}}{\partial z} + \frac{\tau_{rr} - \tau_{\varphi\varphi}}{r} - \sigma B_0^2 u, \tag{3.2}$$

$$\rho\left(u\frac{\partial v}{\partial r} + w\frac{\partial v}{\partial z} + \frac{uv}{r}\right) = \frac{\partial \tau_{r\varphi}}{\partial r} + \frac{\partial \tau_{z\varphi}}{\partial z} + \frac{2\tau_{r\varphi}}{r} - \sigma B_0^2 v, \tag{3.3}$$

27

$$\rho \left(u \frac{\partial w}{\partial r} + w \frac{\partial w}{\partial z} \right) = \frac{\partial \tau_{rz}}{\partial r} + \frac{\partial \tau_{zz}}{\partial z} + \frac{\tau_{rz}}{r}, \tag{3.4}$$

where τ_{ij} $(i, j = 1 - 3)$ are components of stress tensor $\boldsymbol{\tau}$. proposed by Beard and Walters [2] for elastico-viscous liquids (see chapter 1 for details)

Above equations are to be solved for the following constraints:

$$\text{at } z = 0: \quad u = 0, \quad v = r\omega, \quad w = 0, \tag{3.5a}$$

$$\text{as } z \to \infty: \quad u \to 0, \quad v \to 0. \tag{3.5b}$$

The components of stress tensor $\boldsymbol{\tau}$ are obtained from Eq. (1.3) as follows:

$$\tau_{rr} = -P + 2\eta_0 \frac{\partial u}{\partial r} - 2\kappa_0 \left\{ u \frac{\partial^2 u}{\partial r^2} + w \frac{\partial^2 u}{\partial r \partial z} - 2 \left(\frac{\partial u}{\partial r} \right)^2 - \frac{\partial u}{\partial z} \left(\frac{\partial u}{\partial z} + \frac{\partial w}{\partial r} \right) \right\}, \tag{3.6}$$

$$\tau_{\varphi\varphi} = -P + 2\eta_0 \frac{u}{r} - 2\kappa_0 \left\{ \frac{u}{r} \frac{\partial u}{\partial r} - 3 \frac{u^2}{r^2} + \frac{w}{r} \frac{\partial u}{\partial z} - \left(\frac{\partial v}{\partial z} \right)^2 - \left(\frac{\partial v}{\partial r} - \frac{v}{r} \right)^2 \right\}, \tag{3.7}$$

$$\tau_{zz} = -P + 2\eta_0 \frac{\partial w}{\partial z} - 2\kappa_0 \left\{ u \frac{\partial^2 w}{\partial r \partial z} + w \frac{\partial^2 w}{\partial z^2} - \frac{\partial w}{\partial r} \left(\frac{\partial u}{\partial z} + \frac{\partial w}{\partial r} \right) - 2 \left(\frac{\partial w}{\partial z} \right)^2 \right\}, \tag{3.8}$$

$$\tau_{r\varphi} = \eta_0 \left(\frac{\partial v}{\partial r} - \frac{v}{r} \right) - \kappa_0 \left\{ u \frac{\partial^2 v}{\partial r^2} - \left(3 \frac{\partial u}{\partial r} + 2 \frac{u}{r} + w \frac{\partial}{\partial z} \right) \left(\frac{\partial v}{\partial r} - \frac{v}{r} \right) - \frac{\partial v}{\partial z} \left(2 \frac{\partial u}{\partial z} + \frac{\partial w}{\partial r} \right) \right\}, \tag{3.9}$$

$$\tau_{\varphi z} = \eta_0 \frac{\partial v}{\partial z} - \kappa_0 \left\{ u \frac{\partial^2 v}{\partial r \partial z} + w \frac{\partial^2 v}{\partial z^2} - \left(\frac{\partial v}{\partial r} - \frac{v}{r} \right) \left(\frac{\partial u}{\partial z} + 2 \frac{\partial w}{\partial r} \right) - \frac{u}{r} \frac{\partial v}{\partial z} - 3 \frac{\partial v}{\partial z} \frac{\partial w}{\partial z} \right\}, \tag{3.10}$$

$$\tau_{rz} = \eta_0 \left(\frac{\partial u}{\partial z} + \frac{\partial w}{\partial r} \right) - \kappa_0 \left\{ \left(u \frac{\partial}{\partial r} + w \frac{\partial}{\partial z} \right) \left(\frac{\partial u}{\partial z} + \frac{\partial w}{\partial r} \right) - \frac{\partial u}{\partial r} \frac{\partial u}{\partial z} - \frac{\partial w}{\partial r} \frac{\partial w}{\partial z} \right.$$
$$\left. - 3 \left(\frac{\partial u}{\partial z} \frac{\partial w}{\partial z} + \frac{\partial u}{\partial r} \frac{\partial w}{\partial r} \right) \right\}. \tag{3.11}$$

Accounting Eqs. (3.6)-(3.11) and the boundary layer approximations, Eqs. (3.2) and (3.3) become:

$$u \frac{\partial u}{\partial r} + w \frac{\partial u}{\partial z} - \frac{v^2}{r} = \frac{\eta_0}{\rho} \frac{\partial^2 u}{\partial z^2} - \frac{\kappa_0}{\rho} \left\{ \begin{array}{c} u \dfrac{\partial^3 u}{\partial r \partial z^2} + w \dfrac{\partial^3 u}{\partial z^3} - 4 \dfrac{\partial u}{\partial z} \dfrac{\partial^2 u}{\partial z \partial r \partial z} \\[2mm] - \dfrac{\partial u}{\partial r} \dfrac{\partial^2 u}{\partial z^2} - 3 \dfrac{\partial u}{\partial z} \dfrac{\partial^2 w}{\partial z^2} - 2 \dfrac{\partial w}{\partial z} \dfrac{\partial^2 u}{\partial z^2} \\[2mm] - \dfrac{2}{r} \left(\dfrac{\partial u}{\partial z} \right)^2 + \dfrac{2}{r} \left(\dfrac{\partial v}{\partial z} \right)^2 \end{array} \right\} - \frac{\sigma B_0^2}{\rho} u, \tag{3.12}$$

$$u\frac{\partial v}{\partial r} + w\frac{\partial v}{\partial z} + \frac{uv}{r} = \frac{\eta_0}{\rho}\frac{\partial^2 v}{\partial z^2} - \frac{\kappa_0}{\rho}\left\{\begin{matrix} u\dfrac{\partial^3 v}{\partial r\partial z^2} + w\dfrac{\partial^3 v}{\partial z^3} - 2\dfrac{\partial v}{\partial z}\dfrac{\partial^2 u}{\partial r\partial z} \\ -2\dfrac{\partial w}{\partial z}\dfrac{\partial^2 v}{\partial z^2} - 3\dfrac{\partial v}{\partial z}\dfrac{\partial^2 w}{\partial z^2} - \dfrac{6}{r}\dfrac{\partial u}{\partial z}\dfrac{\partial v}{\partial z} \\ -\dfrac{\partial^2 u}{\partial z^2}\left(\dfrac{\partial v}{\partial r} - \dfrac{v}{r}\right) - \dfrac{u}{r}\dfrac{\partial^2 v}{\partial z^2} \end{matrix}\right\} - \frac{\sigma B_0^2}{\rho}v, \tag{3.13}$$

while Eq. (3.4) vanishes identically. For the solution of Eqs. (3.1), (3.2) and (3.3), we use the transformations:

$$u = r\omega F'(\eta), \quad v = r\omega G(\eta), \quad w = -2\sqrt{\omega v}F(\eta), \tag{3.14}$$

with $\eta = z\,(\omega/v)^{1/2}$ assimilarity variable.

With the aid of Eq. (3.14), the mass balance equation (3.1) is fulfilled whereas Eqs. (3.2) and (3.3) give rise to the following ODEs:

$$F''' + G^2 + 2FF'' - F'^2 - K\left(4F'F''' + 2G'^2 - 2FF''''\right) - MF' = 0, \tag{3.15}$$

$$G'' - 2F'G + 2FG' - K(4F'G'' - 2FG''' - 2F''G') - MG = 0, \tag{3.16}$$

and boundary conditions (3.5a) and (3.5b) are transformed as follows:

$$F(0) = 0, \quad F'(0) = 0, \quad G(0) = 1, \tag{3.17a}$$

$$F' \to 0, \quad G \to 0 \text{ as } \eta \to \infty, \tag{3.17b}$$

where $K = k_0\omega/\eta_0$ is the elasticity parameter and $M = \sigma B_0^2/\rho\omega$ is termed magnetic interaction parameter.

3.2   Heat transfer analysis

The difference of temperature between rotating disk and that of fluid serves as a driving potential for heat flow from disk to the fluid. In absence of heat generation/absorption, energy equation takes the following form:

$$\rho C_p\left(u\frac{\partial T}{\partial r} + w\frac{\partial T}{\partial z}\right) = \kappa\left\{\frac{1}{r}\frac{\partial}{\partial r}\left(r\frac{\partial T}{\partial r}\right) + \frac{\partial^2 T}{\partial z^2}\right\} + \Phi, \tag{3.18}$$

where C_p symbolizes specific heat capacity, κ stands for fluid thermal conductivity and Φ represents dissipation function defined as

$$\Phi = \tau_{rr}\left(\frac{\partial u}{\partial r}\right) + \tau_{\varphi\varphi}\left(\frac{u}{r}\right) + \tau_{zz}\left(\frac{\partial w}{\partial z}\right) + \tau_{r\varphi}\left(\frac{\partial v}{\partial r} - \frac{v}{r}\right) + \tau_{\varphi z}\left(\frac{\partial v}{\partial z}\right) + \tau_{rz}\left(\frac{\partial u}{\partial z} + \frac{\partial w}{\partial r}\right). \tag{3.19}$$

Using (3.19) in (3.18) and then simplifying the resulting expression using boundary layer assumptions, one obtains:

$$u\frac{\partial T}{\partial r} + w\frac{\partial T}{\partial z} = \frac{\kappa}{\rho C_p}\frac{\partial^2 T}{\partial z^2} + \frac{\mu}{\rho C_p}\left\{\left(\frac{\partial u}{\partial z}\right)^2 + \left(\frac{\partial v}{\partial z}\right)^2\right\} - \frac{\kappa_0}{\rho C_p}\begin{Bmatrix} u\dfrac{\partial u}{\partial z}\dfrac{\partial^2 u}{\partial r \partial z} + w\dfrac{\partial u}{\partial z}\dfrac{\partial^2 u}{\partial z^2} + \\[1mm] u\dfrac{\partial v}{\partial z}\dfrac{\partial^2 v}{\partial r \partial z} + 3\dfrac{\partial u}{\partial r}\left(\dfrac{\partial v}{\partial z}\right)^2 + \\[1mm] 3\dfrac{u}{r}\left(\dfrac{\partial u}{\partial z}\right)^2 + w\dfrac{\partial v}{\partial z}\dfrac{\partial^2 v}{\partial z^2} - \\[1mm] 3\dfrac{\partial u}{\partial z}\dfrac{\partial v}{\partial z}\left(\dfrac{\partial v}{\partial r} - \dfrac{v}{r}\right) \end{Bmatrix}. \qquad (3.19)$$

We substitute $T = T_\infty + (T_w - T_\infty)\theta(\eta)$, where $\theta(\eta)$ is non-dimensional temperature and wall temperature T_w has the form $T_w = T_\infty + br^2$, in which $b > 0$ is a constant. Eq. (3.19) yields the following ODE:

$$\frac{1}{Pr}\theta'' - 2F'\theta + 2F\theta' + Ec\{F''^2 + G'^2\} - KEc\left\{\begin{matrix} 4F'(F''^2 + G'^2) \\ -2F(F''F''' + G'G'') \end{matrix}\right\} = 0, \qquad (3.20)$$

and boundary conditions for θ are given below:

$$\theta(0) = 1 \text{ and } \theta \to 0 \text{ as } \eta \to \infty. \qquad (3.21)$$

In Eq. (3.20), $Pr = \mu C_p/\kappa$ gives the Prandtl number and $Ec = \omega^2/bC_p$ defines the Eckert number.

In examining von-Kármán boundary layer, an important characteristic is the shear stress experienced at the disk. We define the radial and tangential skin friction coefficients as follows:

$$C_{fr} = \frac{\tau_{rz}|_{z=0}}{\rho(r\omega)^2}, C_{f\theta} = \frac{\tau_{\varphi z}|_{z=0}}{\rho(r\omega)^2}. \qquad (3.22)$$

Upon utilizing Eq.(3.14) and boundary conditions (3.17a) in Eq. (3.22), one arrives at:

$$Re^{1/2}C_{fr} = F''(0), \quad Re^{1/2}C_{f\theta} = G'(0). \qquad (3.23)$$

Another important concept is the Nusselt number defined as $Nu = -Lk(\partial T/\partial z)_{z=0}/\Delta T$ where $L = \sqrt{\nu/\omega}$ denotes the characteristic length. It can be expressed as:

$$Re^{-1/2}Nu = -\theta'(0). \qquad (3.24)$$

Entrainment velocity $w(\infty)$ can be used to determine the amount of fluid sucked towards the disk of radius R as follows:

$$Q = \int_0^R -w(\infty)2\pi r dr = 2\sqrt{v\omega}F(\infty)\pi R^2. \tag{3.25}$$

3.3   Series solution using optimal homotopy analysis method

The detailed solution procedure is discussed in chapter 1 whereas chapter 2 addresses its implementation using a package BVPh 2.0. This problem is solved by making use of the same initial guesses and linear operators as discussed in chapter 2.

3.4.   Results and Discussions

To ascertain that BVPh 2.0 code is working fine, we computed the total average squared residual (defined in chapter 2, Eqs. (2.39)) at different values of K, the elasticity parameter (see Figs. 3.1(a)-3.1(d)). It is apparent that $E_{T,k}$ decreases monotonically as we increase k, the order of approximations. This confirms that obtained series solutions converge to the exact solutions as $k \to \infty$. Having validated the employed method, we now turn to foresee the role of different controlling parameters on the considered model.

The disk surface temperature is assumed to vary quadratically with radial distance r. Such an assumption is necessary for the governing problem to exhibit self-similar solutions. Figs. 3.2a-3.2d include the curves of velocity components and temperature for varying choices of elasticity parameter K. Note that radial velocity ($u = r\omega F'$) and entrained flow are linked in such a way that the radially outflow, produced by centrifugal force, is responsible for drawing the fluid downwards towards the disk. Boundary layer is substantially thinned for increasing K-values. Reduction in radially driven flow by increasing K is noted in Fig. 3.2a. This in turn leads to decelerate the axial fluid motion and thus the volumetric flow rate. No overshoot in similarity profiles is detected for the considered range of K. Circumferential flow is predicted to accelerate whenever elastic effects are considered (see Fig 3.2c). On the contrary, fluid temperature rises for increasing K-values.

To see how present flow model is influenced by the presence of magnetic field, we prepared Figs. 3.3(a)-3.3(d) showing velocity and temperature curves for a variety of M-values. It is noted that asymptotic value of F, that is $F(\infty)$, decreases for increasing values of M. Also, it takes shorter distances from the disk for the velocity profiles to attain their respective asymptotic values as M is increased. Moreover, u-velocity profile ($u = r\omega F'$) becomes flatter for higher

values of M. Furthermore, the resistance offered to fluid motion by the Lorentz force leads to enhancement in temperature profile as apparent from Fig. 3.3(d).

Fig. 3.4(a) shows the change in temperature distribution by varying Pr, the Prandtl number. It takes smaller distances from the disk for temperature curve to reach η-axis for increasing Pr-values. Moreover, the effect of Eckert number Ec is seen to be typical of fluid gaining temperature (due to the loss of heat energy from the disk) (see Fig. 3.4(b)).

In Figs. 3.5a-3.5d, we present the graphs of $Re^{1/2}C_{f_r}, Re^{1/2}C_{f_\theta}, Re^{-1/2}Nu$ and $F(\infty)$ against the elasticity parameter K for the values of latter in the range 0 to 1. While the results reveal that radial skin friction can be lowered by including elastic effects, the azimuthal skin friction first decreases to a minimum and then increases as K increases. Nusselt number, measuring heat transfer rate, is predicted to elevate whenever K enlarges. Interestingly, $F(\infty)$ has an inversely linear profile against both K and M. Both radial and azimuthal wall stresses exhibit increasing trends for increasing values of K.

Table 3.1 contains the numerical data of entrainment velocity, radial wall stress and tangential wall stresses by changing the values of K and M. Axial velocity at infinity, measuring the volume of entrained fluid is lowered whenever K or M is incremented. This reduction signals a growth in velocity gradients at the surface which yields higher magnitude of skin friction coefficients. Hence, we conclude that larger torque at the disk is required whenever elasticity and magnetic field effects are present.

Numerical data exhibiting the effect of involved physical parameters on Nusselt number is tabulated (see Table 3.2). For higher Pr-values, heat convection measuring heat transfer rate from the surface is significant relative to pure conduction. Hence, Nusselt number increases in absolute sense for increasing values of Pr. Heat dissipation due to fluid friction strengthens as Ec becomes large. This in turn yields expansion in temperature profile and reduction in Nusselt number. Figs. 3.2a already indicated a clear reduction in axial velocity whenever elastico-viscous fluid is considered. Thus magnitude of the term $w\partial T/\partial z$ (in Eq. (3.19)), measuring heat convection, reduces when K is enhanced. As a result, Nusselt number is seen to lower substantially when K enlarges. Similar conclusion can be made for the influence of magnetic force on Nusselt number.
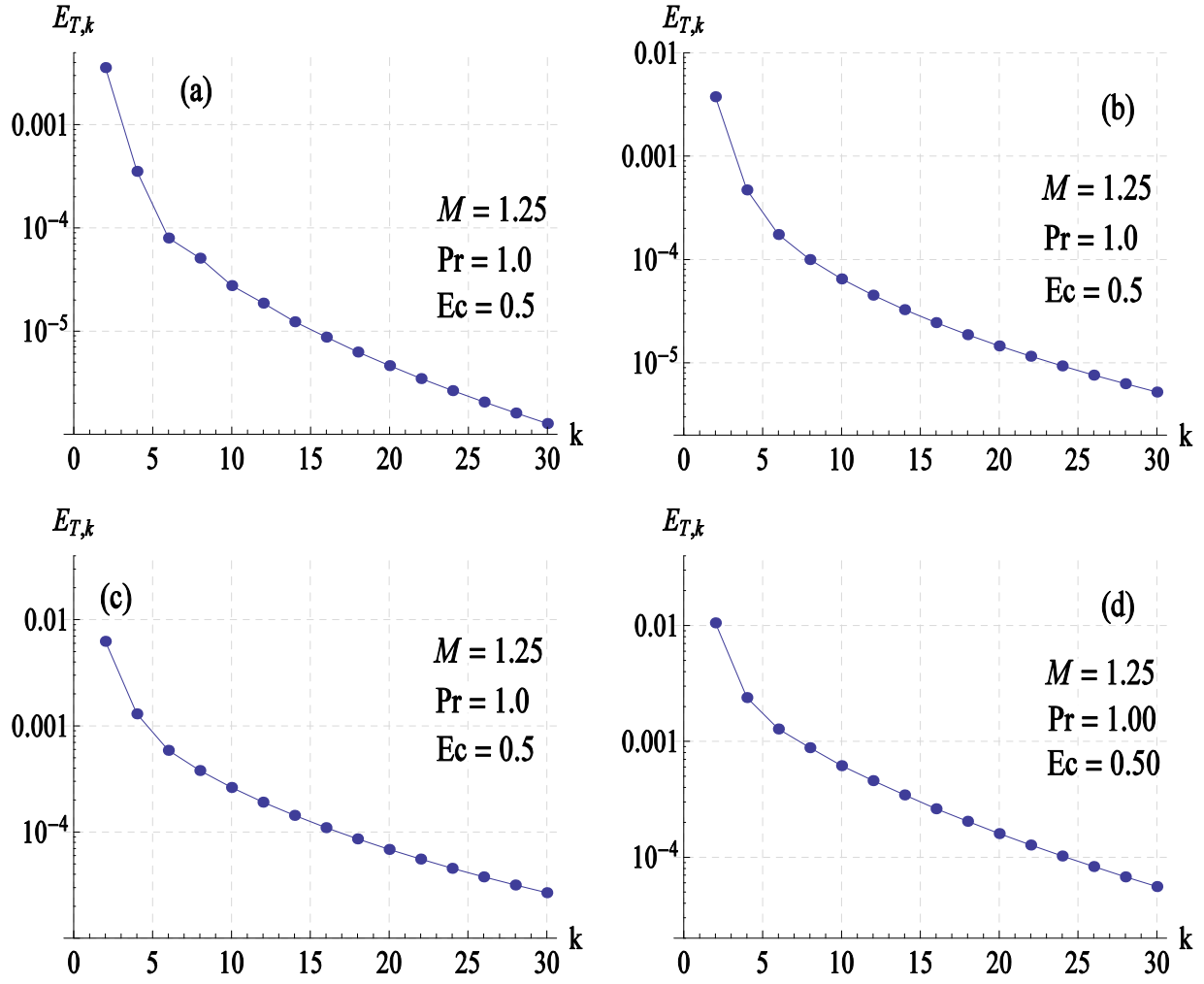
Fig. 3.1: Total residual error ($E_{T,k}$) versus order of approximations (k) at (a) $K = 0$, (b) $K = 0.25$, (c) $K = 0.5$ and (d) $K = 0.8$.
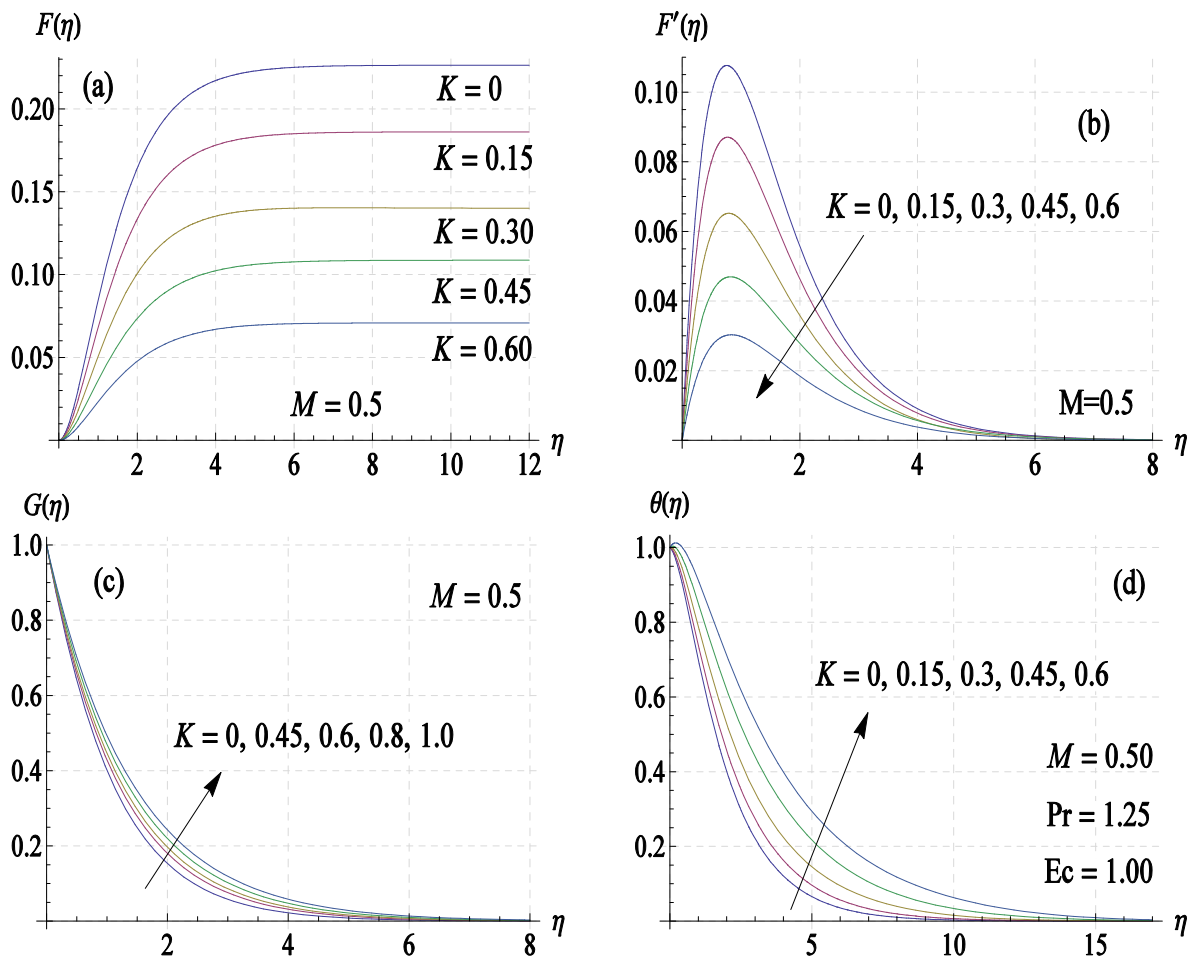
Fig. 3.2: Curves of velocity components (F, F', G) and temperature (θ) for varying choices of elasticity parameter K.
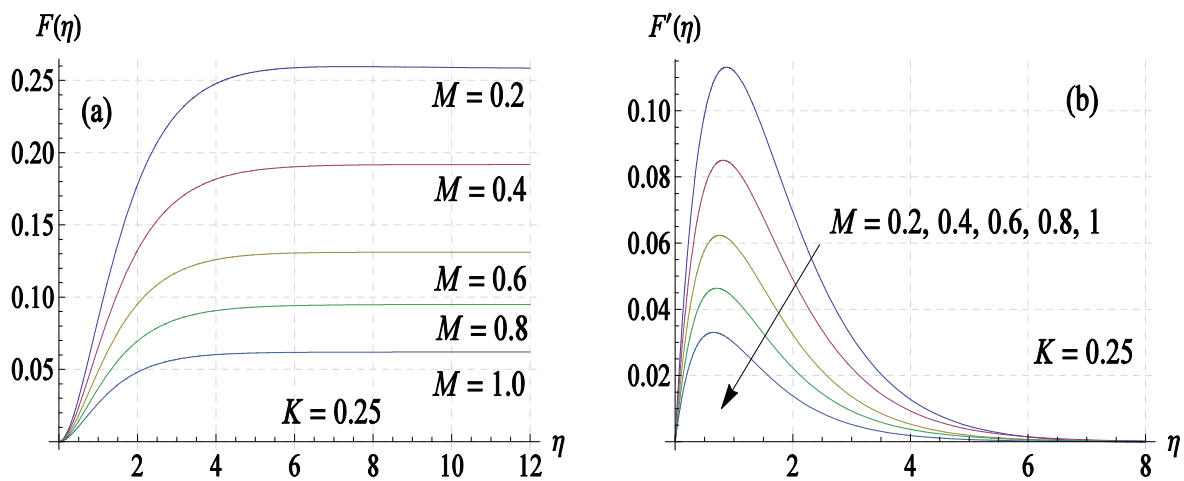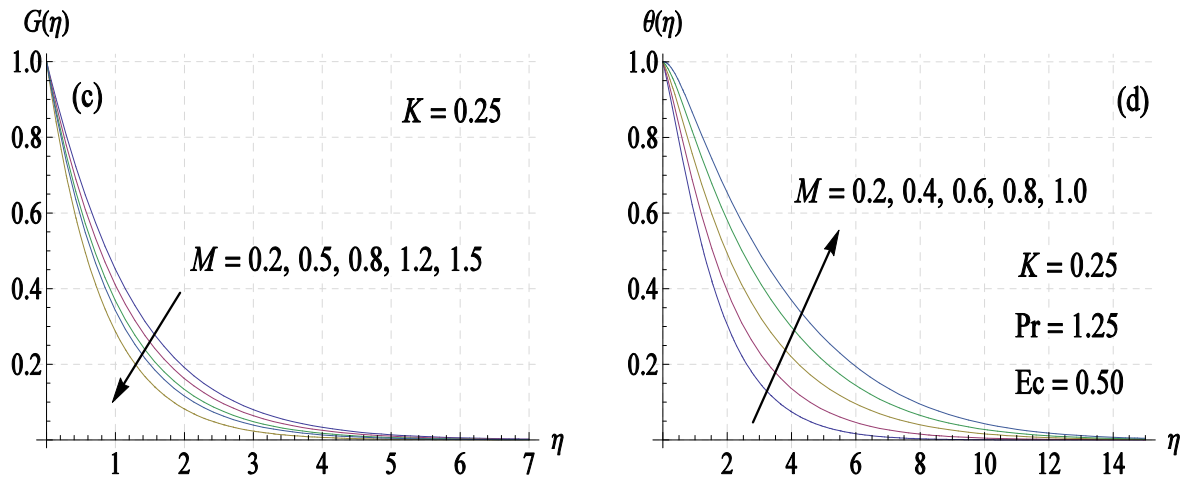
Fig. 3.3: Change in velocities (F, F', G) and temperature (θ) against η for varying choices of magnetic interaction parameter M.
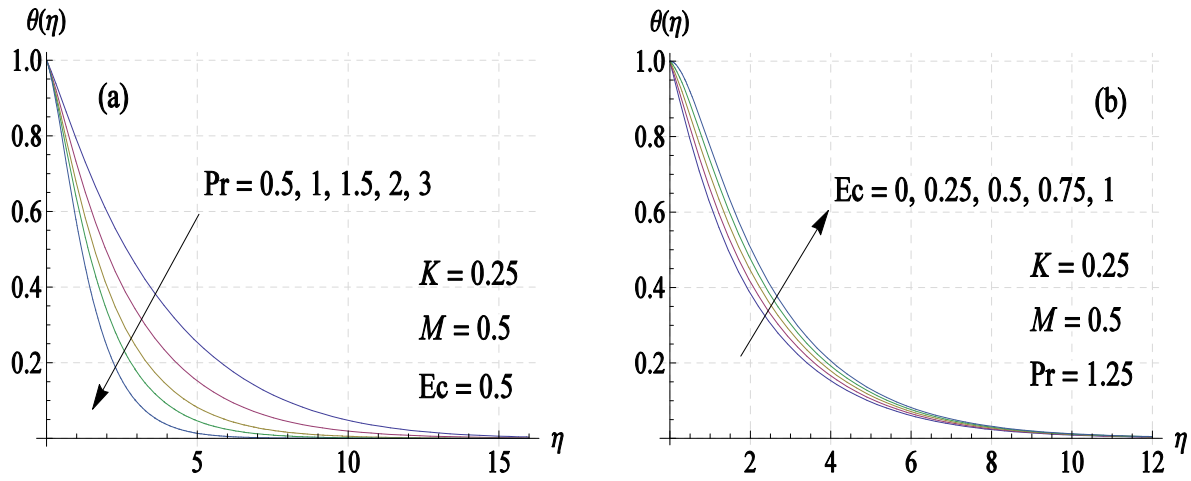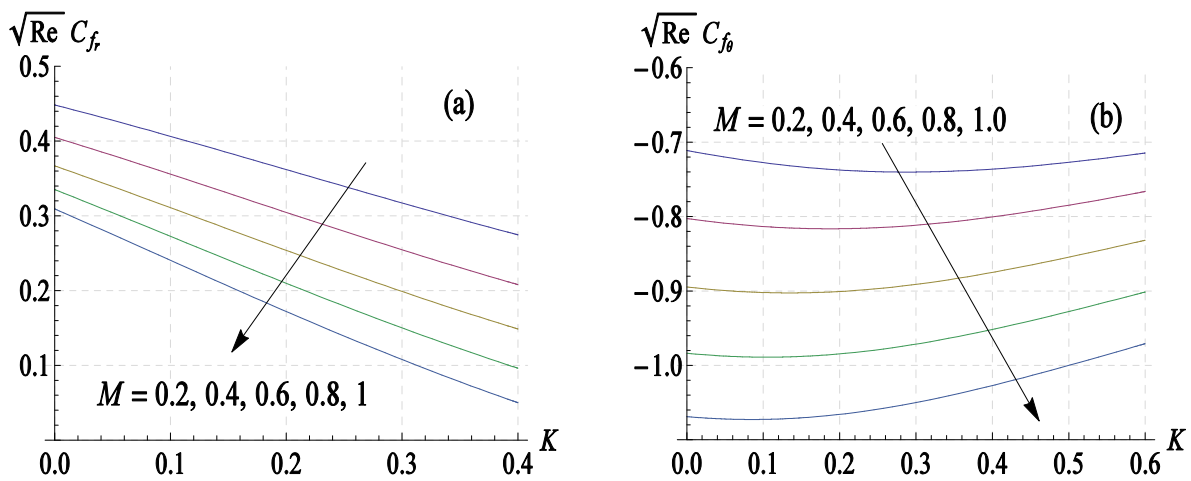

Fig. 3.4: Change in fluid temperature $\theta(\eta)$ against vertical distance η for varying choices of (a) Prandtl number Pr and (b) Eckert number Ec.
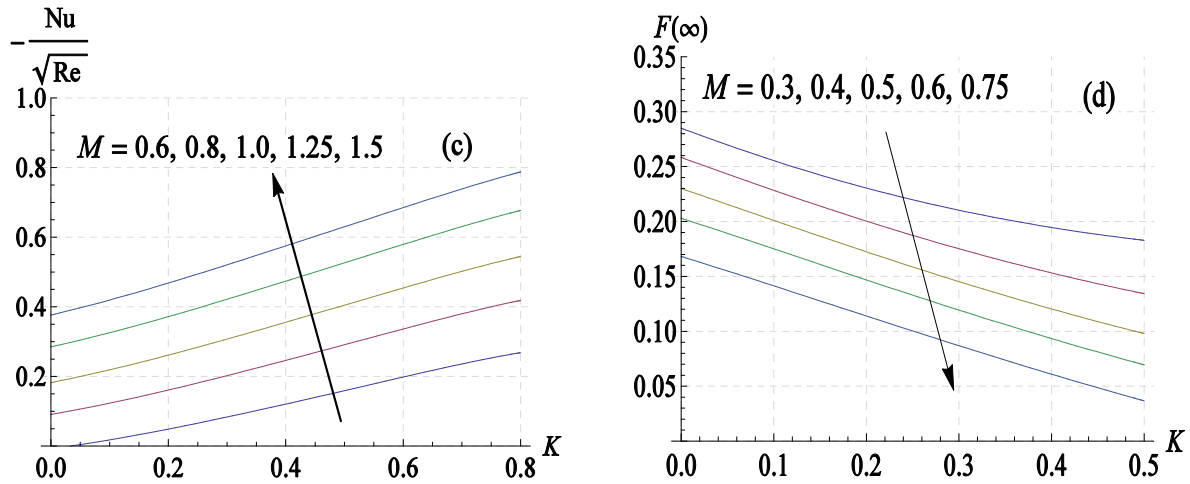
Fig. 3.5: Profiles of skin-friction coefficients, Nusselt number and volume flow rate versus elasticity parameter K for varying choices of M.

Table 3.1: Numerical results of skin-friction coefficients for varying choices of K and M at 20th-order of approximations.

K	M	$F(\infty)$	$Re^{\frac{1}{2}}C_{f_r}$	$Re^{\frac{1}{2}}C_{f_\theta}$
0.2	0.5	0.175165	0.279125	-0.857647
0.3		0.147619	0.226650	-0.850164
0.4		0.122389	0.178885	-0.835553
0.5		0.097984	0.136315	-0.816793
0.2	0.2	0.295671	0.368621	-0.728808
	0.5	0.175165	0.279125	-0.857647
	0.8	0.104394	0.209732	-0.984472
	1.2	0.052581	0.139514	-1.144154

Table 3.2: Computational results of Nusselt number for a varying choices of K, M, Pr and Ec at 20th-order of approximations.

K	M	Pr	Ec	$-\theta'(0)$
0	0.5	1.25	0.5	0.295399
0.2				0.228719
0.4				0.145372
0.6				0.057209
0.2	0.2			0.380507
	0.4			0.280761
	0.6			0.176379

36

Table 3.2 *(continued)*

K	M	Pr	Ec	$-\theta'(0)$
	1.0			0.008257
	0.5	0.5		0.167541
		0.75		0.193142
		1.00		0.213086
		1.25		0.228719
		1.25	0	0.451032
			0.30	0.316919
			0.70	0.139779
			1.00	0.006359

3.5. Concluding remarks

In this framework, we discussed elastico-viscous fluid flow bounded by uniformly rotating disk considering heat dissipation effects. Present analysis is based on a quadratic surface temperature distribution which is prerequisite for achieving self-similar solution. The developed system of equations is treated via package BVPh 2.0 of MATHEMATICA based on the HAM. The specific conclusions of the present study are outlined as follows:

- Using the package BVPh 2.0, the averaged squared residual of the governing system is computed which reflects that series solutions converge to the exact solutions as k (order of approximation) tends to infinity.

- Akin to earlier works (see, for instance, [44] and [46]),an increase in elasticity parameter K has an retarding effect on the boundary layer flow. The entrained volume of the fluid upon the disk also decreases with an enhancement in elasticity.

- The effect of elasticity is such that radial wall stress decreases as values of K are incremented. However, the resisting torque first decreases to a minimum and then increases for increasing K-values. Notably, for sufficiently higher values of M, resisting torque is monotonically increasing function of K.

- An expansion in thermal boundary layer is found for increasing values of K. Such increase accompanies with reduced heat transfer rate from the rotating surface.

- The existence of axial magnetic field opposes the flow of fluid in radially outward direction initiated by centrifugal force. Such opposition restricts the amount of fluid drawn vertically thereby providing an expansion in temperature profile.

- As we increase the Eckert number, a relative decrease in enthalpy is noticed which in turn leads to an enhancement in the temperature profile.

References

1. R. S. Rivlin, J. L. Ericksen, Stress deformation relations for isotropic materials, J. Rat. Mech. Anal. 4 (1955), 323-425.

2. D. W. Beard, and K. Walters, Elastico-viscous boundary layer flows. Part I. Two-dimensional flow near a stagnation point, Proc. Camb. Phil.Soc. 60 (1964), 667-674.

3. K. R. Rajagopal, T. Y. Na and A. S. Gupta, Flow of a viscoelastic fluid over a stretching sheet, Rheol. Acta 23 (1984) 213-215.

4. B. S. Dandapat and A. S. Gupta, Flow and heat transfer in a viscoelastic fluid over a stretching sheet, Int. J. Non-Linear Mech. 24 (1989) 215-219.

5. M. S. Sarma and B. N. Rao, Heat transfer in a viscoelastic fluid over a stretching sheet, J. Math. Analy. &Applicat. 222 (1998) 268-275.

6. K. Vajravelu and D. Rollins, Hydromagnetic flow of a second grade fluid over a stretching sheet, Appl. Math. &Comput. 30 (2004) 783-791.

7. K. Sadeghy and M. Sharifi, Local similarity solution for the flow of a "second-grade" viscoelastic fluid above a moving plate, Int. J. Non-Linear Mech. 39 (2004) 1265-1273.

8. R. Cortell, Toward an understanding of the motion and mass transfer with chemically reactive species for two classes of viscoelastic fluid over a porous stretching sheet, Chem. Eng. & Process. - Process Intensific. 46 (2007) 982-989.

9. Z. Abbas, Y. Wang, T. Hayat and M. Oberlack, Hydromagnetic flow in a viscoelastic fluid due to the oscillatory stretching surface, Int. J. Non-Linear Mech. 43 (2008) 783-793.

10. B. Sahoo. Effects of partial slip on axisymmetric flow of an electrically conducting viscoelastic fluid past a stretching sheet, Cent. Euro. J. Phy. 8 (2010) 498–508.

11. J. C. Mishra, G. C. Shit, S. Chandra and P. K. Kundu, Hydromagnetic flow and heat transfer of a second-grade viscoelastic fluid in a channel with oscillatory stretching walls: application to the dynamics of blood flow, J. Eng. Math. 69 (2011) 91-100.

12. M. Turkyilmazoglu, Multiple solutions of hydromagnetic permeable flow and heat for viscoelastic fluid, J. Thermophys. & Heat Transf. 25 (2011), doi: 10.2514/1.T3749.

13. S. Abbasbandy and T. Hayat, On series solution for unsteady boundary layer equations in a special third grade fluid, Commun. Nonlinear Sci. &Numer. Simul. 16 (2011) 3140-3146.

14. B. Sahoo and S. Poncet, Flow and heat transfer of a third grade fluid past an exponentially stretching sheet with partial slip boundary condition, Int. J. Heat & Mass Transf. 54 (2011) 5010-5019.

15. M. Turkyilmazoglu, Three dimensional MHD flow and heat transfer over a stretching/ shrinking surface in a viscoelastic fluid with various physical effects, Int. J. Heat & Mass Transf. 78 (2014) 150-155.

16. K. Naganthran, R. Nazar and I. Pop, Unsteady stagnation-point flow and heat transfer of a special third grade fluid past a permeable stretching/shrinking sheet, Sci. Rep.6(2016), Article ID: 24632.

17. M. Mustafa, Viscoelastic flow and heat transfer over a nonlinearly stretching sheet: OHAM solution, J. Appl. Fluid Mech. 9 (2016) 1321-1328.

18. B. Marinca and V. Marinca, Some exact solutions for MHD flow and heat transfer to modified second grade fluid with variable thermal conductivity in the presence of thermal radiation and heat generation/absorption, Comput. & Math. Applicat. 76 (2018) 1515-1524.

19. T. von Kármán, Überlaminare und turbulenteReibung, Zeitschrift fur Angew. Math. Mech. ZAMM 1 (1921) 233-252.

20. W. G. Cochran, The flow due to a rotating disk, Proceedings of the Cambridge Philosophical Society 30 (1934) 365–375.

21. K. Millsaps and K. Pohlhausen, Heat transfer by laminar flow from a rotating disk, J. Aeronaut. Sci. 19 (1952) 120–126.

22. J. A. D. Ackroyd, On the steady flow produced by a rotating disk with either surface suction or injection, J. Eng. Math. 12 (1978) 207–220.

23. H. A. Attia, Unsteady MHD flow near a rotating porous disk with uniform suction or injection, Fluid Dynam. Res. 23 (1998) 283-290.

24. H. S. Takhar, A. K Singh and G. Nath, Unsteady MHD flow and heat transfer on a rotating disk in an ambient fluid, Int. J. Therm. Sci. 41 (2002) 147-155.

25. P. D. Ariel, On computation of MHD flow near a rotating disk, ZAMM-J. Appl. Math. & Mech. 82 (2002) 235-246.

26. M. Miklavcic and C. Y. Wang, The flow due to a rough rotating disk, Z. angew. Math. Phys. 54 (2004) 1-12.

27. H. Xu and S. J. Liao, A series solution of the unsteady von-Kármán swirling viscous flows, Acta Appl. Math. 94 (2006) 215–231.

28. T. Fang, Flow over a stretchable disk, Phys. Fluids 19 (2007) https://doi.org/10.1063/1.2823572.

29. H. A. Attia, The effect of ion-slip on the flow of Reiner-Rivlin fluid due to a rotating disk with heat transfer, J. Mech. Sci. & Tech. 21 (2007) 174-183.

30. M. Turkyilmazoglu, Exact solutions for the incompressible viscous fluid of a porous rotating disk flow, Int. J. Non-Linear Mech. 44 (2009) 352-357.

31. M. Turkyilmazoglu, Three dimensional MHD stagnation flow due to a stretchable rotating disk, Int. J. Heat & Mass Transf. 55 (2012) 6959-6965.

32. Ahmadpour and K. Sadeghy, Swirling flow of Bingham fluids above a rotating disk: An exact solution, J. Non-Newtonian Fluid Mech. 197 (2013) 41-47.

33. M. Turkyilmazoglu and P. Senel, Heat and mass transfer of the flow due to a rotating rough and porous disk, Int. J. Therm. Sci. 63 (2013) 146-158.

34. P.T. Griffiths, Flow of a generalized Newtonian fluid due to a rotating disk, J. Non-Newtonian Fluid Mech. 221 (2015) 9-17.

35. Guha and S. Sengupta, Analysis of von Kármán's swirling flow on a rotating disc in Bingham fluids, Phys. Fluids 28 (2016) https://doi.org/10.1063/1.4937590.

36. Mustafa, T. Javed and A. Ghaffari, Heat transfer in MHD stagnation point flow of a ferrofluid over a stretchable rotating disk, J. Molec. Liq. 219 (2016) 526-532.

37. J. A. Khan, M. Mustafa, T. Hayat and A. Alsaedi, A revised model to study the MHD nanofluid flow and heat transfer due to rotating disk: numerical solutions, Neural Comput. &Applicat. (2016) https://doi.org/10.1007/s00521-016-2743-4.

38. D. H. Doh and M. Muthtamilselvan, Thermophoretic particle deposition on magnetohydrodynamic flow of micropolar fluid due to a rotating disk, Int. J. Mech. Sci. 130 (2017) 350-359.

39. M. Mustafa and J. A. Khan, Numerical study of partial slip effects on MHD flow of nanofluids near a convectively heated stretchable rotating disk, J. Mol. Liq. 234 (2017) 287-295.

40. M. Turkyilmazoglu, Fluid flow and heat transfer over a rotating and vertically moving disk, Phys. Fluids 30 (2018) Article ID 063605, doi:https://doi.org/10.1063/1.5037460.

41. M. Mustafa, M. Tabassum and M. Rahi, Second law analysis of heat transfer in swirling flow of Binghamfluid by a rotating disk subjected to suction effect, Thermal Science (2019), doi: https://doi.org/10.2298/TSCI180722162M.

42. S. M. R. S. Naqvi, T. Muhammad, S. Saleem and H. M. Kim, Significance of non-uniform heat generation/absorption in hydromagnetic flow of nanofluid due to stretching/shrinking disk, Physica A (2019), In Press;(https://doi.org/10.1016/j.physa.2019.123970)

43. M. Asma, W. A. M. Othman and T. Muhammad, Numerical study for Darcy–Forchheimer flow of nanofluid due to a rotating disk with binary chemical reaction and Arrhenius activation energy, Mathematics 7 (2019);https://doi.org/10.3390/math7100921.

44. L. Elliott, Eiastico-viscous flow near a rotating disk. Phys. Fluids 14 (1971) 1086-1090.

45. P. D. Ariel, Computation of flow of a second grade fluid near a rotating disk, Int. J. Eng. Sci. 35, (1997) 1335-1357.

46. P. D. Ariel, On the flow of an elastico-viscous fluid near a rotating disk, J. Comput. & Appl. Math. 154 (2003) 1-25.

47. M. Imtiaz, A. Kiran, T. Hayat and A. Alsaedi, Joule heating and MHD effects in flow ofsecond-grade fluid due to a rotating diskwith variable thickness, Phys. Scr. 94 (2019) Article ID 085203, doi:https://doi.org/10.1088/1402-4896/ab0607.

48. S. J. Liao, An optimal homotopy analysis approach for strong nonlinear differential equations, Commun. Nonlinear Sci. &Numer. Simulat. 15 (2010) 2003-2016.

49. U. Farooq, Y. L. Zhao, T. Hayat, A. Alsaedi and S. J. Liao, Application of the HAM-based Mathematica package BVPh 2.0 on MHD Falkner-Skan flow of nano-fluid, Comput. & Fluids 111 (2015) 69-75.

50. S. Liao, Advances in the homotopy analysis method, World Scientific (2013).

51. M. Ramzan, M. Bilal, U. Farooq and J. D. Chung, Mixed convective radiative flow of second grade nanofluid with convective boundary conditions: An optimal solution, Res. Phys. 6 (2016) 796-804.

52. T. Hayat, F. Haider, T. Muhammad and A. Alsaedi, Three dimensional rotating flow of carbon nanotubes with Farcy-Forchheimer porous medium, PLOS ONE 12 (2017).https://doi: 10.1371/journal.pone.0179576.